Structures 69 (2024) 107348

Contents lists available at ScienceDirect

Structures

journal homepage: www.elsevier.com/locate/structures

Modeling of in-plane floor flexibility in existing reinforced concrete buildings

Simone Baldassi [a,*], Igino Pitacco [a], Giada Frappa [a], Fabio Rizzo [b], Margherita Pauletta [a]

[a] Polytechnic Department of Engineering and Architecture, University of Udine, Via delle Scienze 206, 33100 Udine, Italy
[b] Department of Architecture, Construction and Design, Polytechnic of Bari, via Orabona 4, 70125 Bari, Italy

ARTICLE INFO

Keywords:
Flexible floor system
Orthotropic slab
Existing RC buildings
Seismic analysis
Finite element analysis
Homogenization method

ABSTRACT

The paper addresses the problem of determining the mechanical characteristics of an orthotropic slab that best represents the in-plane behavior of a complex reinforced concrete (RC) floor system. To represent the structural behavior of the real RC floor, a reference model composed of solid finite elements is developed. The mechanical parameters of the equivalent orthotropic slab are determined by different homogenization techniques. In particular, two numerical algorithms and an analytical procedure to derive the elastic parameters of the equivalent slab representing the in-plane behavior of a single floor cell are proposed. Then, to determine which homogenization technique best predicts the structural behavior, representative one-story and six-story structures are modeled using both the equivalent slabs obtained using the three proposed techniques and the reference floor model. A discussion of the suitability of modeling floor in-plane flexibility taking account of only the top RC slab, for the considered case studies, is also provided.

1. Introduction

The response of multi-story buildings to horizontal forces (earthquake and wind) is strongly influenced by the in-plane floor stiffness.

In general, the greater the floor stiffness, the more the horizontal forces are transferred to vertical resisting elements proportionally to their lateral stiffness, with the limit case being infinitely rigid floors (rigid diaphragms). Experimental and computational studies on Reinforced Concrete (RC) wall structures and masonry structures with timber or steel floors have shown the great influence of floor flexibility on structural response to seismic loads [1–12].

Among these studies Tena-Colunga et al. [10,11] carried out pioneering research about orthotropic floors in a low-rise masonry structure. By means of a Finite Element Model (FEM), these authors studied the structural behavior of the firehouse of Gilroy, located about 15 km from the main shock epicenter of 1989 Loma Prieta Earthquake. The structure was also instrumented in order to assess the reliability of the FEM. In the first article [10], the authors found that quasi-dynamic analysis is reliable and has a low computational cost, however it is not the best choice for complex building models. Time step integration analysis is still a valid analysis approach. In the second article [11], the authors found that a simplified multi-degree of freedom linear dynamic analysis can represent the structural behavior more efficiently than FEM.

Several studies investigated the influence of some characteristics of the building configuration on how floor flexibility affects the response of the RC structures. Saffarini et al. [13] carried out a parametric study on 37 buildings, by varying number of stories, story height, slab type, building plan aspect ratio, plan regularity, openings in the slab, and sizes and spacing of columns or shear walls. These authors showed that floor flexibility has a great effect on the structural behavior in the presence of shear walls, and that this effect depends on the ratio between the floor in-plane stiffness and the stiffness of the lateral load resisting system decreases. Conversely, in framed RC structures the errors introduced by the rigid diaphragm assumption were negligible.

Ruggieri et al. [14] investigated the effects of floor deformability in existing RC buildings, in particular on the structural behavior and the seismic fragility of the structure. The authors developed a practical procedure to provide an a priori definition of the floor deformability. The authors analyzed two existing buildings and found that the behavior of these buildings is more and more flexible by increasing the stiffness of the structural vertical system.

Tena-Colunga et al. [15] assessed the effects of in-plane floor flexibility in multi-story buildings, considering different floor systems and

* Corresponding author.
E-mail address: baldassi.simone@spes.uniud.it (S. Baldassi).

https://doi.org/10.1016/j.istruc.2024.107348
Received 16 January 2024; Received in revised form 5 August 2024; Accepted 20 September 2024
Available online 3 October 2024

variable plan aspect ratios. The study determined that RC waffle flat slab is the most flexible floor system among those investigated in the paper, with an average peak lateral displacement 1.9 times higher than those for rigid diaphragm buildings, whereas the precast beam and block floor system is the stiffest. The ribbed RC slab floor system displays an average peak lateral displacement of 1.8 times higher than those for rigid diaphragm buildings. The study also concluded that a well-designed floor system, fulfilling code regulations, can result in floor systems that behave like rigid diaphragms, especially for buildings where the bay widths are not very large.

Ju et al. [16] compared the results achieved by framed and shear wall structures with T-, U- or rectangular-shaped buildings, obtained using both a rigid diaphragm assumption and flexible-floor analyses. The article highlighted that for buildings with shear walls, analysis results for the rigid-floor model can differ greatly from those of flexible-floor analyses, due to the very large lateral stiffness of the shear wall system.

Basu et al. [17] developed a formulation to predict the horizontal forces distribution among vertical structural members and the accidental torsion in asymmetrical structures with flexible floors, where the torsional amplification can be quite significant.

Fang et al. [18] compared the behavior of symmetric and asymmetric steel structures with rigid or semi-rigid diaphragms considering also the influence of vertical elements inelasticity on the structure torsional behavior. These authors found that the inelastic behavior of the lateral load resisting system significantly affects the torsional irregularity of the structures. Furthermore, they assessed that the relative rotation angle and inter-story drift ratio are higher for buildings with semi rigid diaphragms than for those with rigid diaphragms.

Tena-Colunga et al. [19] investigated the behavior of existing buildings characterized by in-plan irregularity. The authors analyzed two multi-story buildings with floors made of flat slab systems and lightening EPS blocks, modeling the entire structure by means of solid finite elements. The authors remarked the necessity of taking into account the in-plane flexibility for this kind of floor, since they found an increase in the lateral displacements and natural periods of vibration when with respect to the rigid floors models. Furthermore, the authors found that plan irregularity plays and important role in in-plane floor flexibility, and that the presence of large reentrant corners and floor openings can reduce the strength of the floor system.

Eivani et al. in [20] analyzed the floor flexibility effect on plan-asymmetric RC structures. The paper identified a reduction in rigid body motion and an amplification in bending and shear deformation of the floor when the diaphragm flexibility is increased.

Sadashiva et al. [21] investigated the influence of floor flexibility on building vibration modes. The paper determined that fundamental natural period of structures with flexible diaphragms is always greater than that of those with rigid diaphragms. The authors also developed a simple equation to estimate the fundamental natural period of a structure with flexible diaphragms.

The simultaneous effects of seismic action intensity and floor flexibility were analyzed in [22]. The paper determined a reduction of the torsional deformation of buildings with flexible floors and highlighted the necessity to consider strength and deformability checks of the floor elements.

Masi et al. [23] analyzed a two-story building with different shear wall configurations, also determining the ductility demand of walls and floor elements. These authors demonstrated that the rigid floor design hypothesis leads to mean values of ductility demand consistently lower than those obtained with the flexible floor hypothesis. Furthermore, they stated that an inadequate floor strength produces considerable plastic floor deformation in the floor and a significant reduction in the ductility demand of vertical elements.

Both Khajehdehi et al. [24] and Kalib et al. [25] investigated the influence of openings on flexibility of RC floor slabs, analyzing also crack development and slab collapse. The first study [24] revealed that the presence of openings in the floor slab leads to a different failure mechanism than that of a slab without openings. The second study [25] instead reported a decrease in lateral displacement with increasing size of openings in flat floor slabs. Furthermore, slabs without openings showed high inelastic deformation compared to slabs with openings.

Fleischman et al. [26] and Kunnath et al. [27] analyzed the effect of floor inelasticity on the structure response. The first study [26] determined that the building demand is higher at lower stories. Elastic diaphragm structures have a higher force demand at lower stories, whereas inelastic diaphragm structures have a higher deformation demand at lower stories. The second study [27] assessed that, compared to values predicted using the rigid diaphragm assumption, there is a larger strength and ductility demand on the vertical elements near the area in which inelastic floor deformation occurs.

Despite plenty of studies confirming the need to take into account floor flexibility, the rigid floor assumption is commonly adopted by engineers, due to great modeling and computational simplifications. Fortunately, the shortcomings of this assumption are mitigated by building code recommendations [28–34], which provide qualitative and/or quantitative criteria to assess its suitability. For instance, a qualitative criterion in Eurocode 8 [28] sets a minimum slab thickness of $4cm$ in ribbed RC floors and a maximum floor plan aspect ratio of $4:1$ to allow the adoption of rigid diaphragm assumption. Quantitative criteria are based on the limitation to floor in-plane displacements. For instance, the same Eurocode 8 allows the floors to be considered rigid if the in-plane displacement differences between the flexible floor model and the rigid diaphragm model are less than 10%.

Since floor flexibility must be always considered, at least in preliminary structural analyses to verify if the rigid diaphragm assumption can be adopted, there is the need for a simple but accurate way to represent the in-plane behavior of complex floor systems. In this paper the focus is on the one-way joist floor system (see Fig. 1), widely adopted in existing RC Italian, European buildings but also worldwide, as seen in [19], consisting of a monolithic combination of a grid of RC beams, regularly spaced joists, a top slab and lightweight elements between the joists, as detailed in Section 2.1.

A possible and widespread simplified approach is to represent the complex floor system with a uniform orthotropic slab superimposed on the grid of RC beams discretized by flat shell Finite Elements (FE). In order to assess the effect of the floor in-plane flexibility on the distribution of shear forces among vertical structural members before plastic deformation occurs the floor elastic behavior is considered. The determination of the orthotropic slab properties is dealt with by the homogenization theories.

The homogenization of stiffened plates (e.g. ribbed or corrugated) is a longstanding problem, as it can be seen from the introduction of Trotsky's monograph [35], where a bibliography on the topic updated to the 1970s is presented. Although the topic of homogenization has received much attention over the years, due to the great diffusion of composite materials products, its application to reinforced concrete floor systems is not so widespread.

In this regard, particularly interesting are the works of Staszak et al. [36,37], in which an elegant method of numerical homogenization,

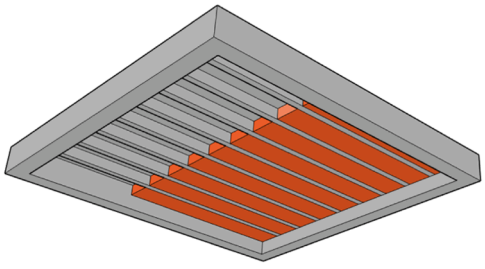

Fig. 1. Graphical perspective of a floor cell.

originally proposed by Biancolini [38] for corrugated boards, is applied to prefabricated composite wide slabs [36] and to bubble deck concrete slabs [37]. In this method a Representative Volume Element (RVE) of the deck is modeled in great detail by 3D FEs, and its stiffness matrix is reduced by static condensation so that only the Degree of Freedom (DoF) of the outer RVE boundary survives. Then a uniform strain kinematic boundary condition is imposed on the RVE boundary, to get a stiffness matrix relating the boundary traction to the uniform strain tensor, which allows one to equate the elastic energy of the RVE to that of the orthotropic equivalent shell element.

Another approach is that proposed by Pecce et al. [39] and Ruggeri et al. [40], which consists of assigning the elastic properties of concrete to the equivalent (orthotropic) slab, leaving only the slab thickness free to match as close as possible the behavior of the reference floor modeled by solid FEs. The first orthotropic model to study the in-plane flexibility of a RC floor system (precast beam and block system) was proposed by Tena-Colunga et al. in [15]. The model was also adopted in [19] to reproduce the in-plane flexibility of a lightened RC floor system in medium-rise RC and confined masonry buildings with irregular plan. The difference between these two recent studies lies in the boundary conditions imposed to the floor FE model.

Conversely, other studies determined the mechanical properties of materials and building elements though experimental data. Among the latest research, Foti et al. [41] instrumented an existing building to record the structure vibrational modes due to environmental noise. The authors then developed a FEM to carry out the modal analysis of the building. The comparison of the vibrational modes obtained from the FEM and those recorded by the instrumentation, allowed to determine the mechanical properties of the FEM structure elements.

In this paper the approach described in [39,40] is extended by evaluating the whole set of mechanical properties of the equivalent orthotropic floor slab, by representing the behavior of a single floor cell by means of three different homogenization techniques proposed herein and described in Section 3. The main novelty aspects introduced by this research work lie in the proposal of three different homogenization techniques to be applied to single floor cells. Conversely, in [39] and [40] the behavior of the whole floor is analyzed. In particular, a new analytical technique and two new numerical algorithms are proposed to determine the elastic parameters of the equivalent orthotropic slab. To determine which of the proposed techniques provides the most realistic results, structural analyses were carried out on two simple one-story buildings and two six-story buildings. The results of the analyses obtained with the different homogenization techniques are compared to those obtained from the reference FE model, in which the floors are modeled accurately with solid finite elements, and also to those obtained by the rigid diaphragm assumption. The comparison is done in terms of both horizontal displacements and shear in the columns, and it is discussed in Sections 4 and 5 for the one-story and six-story buildings, respectively. The suitability of modeling floor in-plane flexibility taking account of only the top RC slab, a common practice, is also discussed.

Only the elastic behavior is considered herein, because even during the elastic stage, displacements and shear acting on the vertical elements are influenced by the floor flexibility. When yielding occurs in the floor and/or in the vertical elements, the forces have already been distributed according to certain rates, which depend on the initial stiffness of the structure elements.

The research significance of the present study is to provide practitioners with a useful tool to model the in-plane floor flexibility in a simple but as accurate way as possible, in order to realistically assess the distribution of seismic forces among the vertical structural elements. This is very important to correctly design these elements and prevent unexpected collapses.

Moreover, flexible RC floors are often found in existing buildings. Increasingly frequently, in the last decades, the seismic retrofit of these buildings has been made with steel braces, easy to install and effective in capturing part of the seismic force acting on the building. The steel braces behave like shear walls; hence their presence may amplify the effects due to flexible floors and reduce the effectiveness of the braced reinforcing system.

Finally, to investigate the effect of in-plane floor flexibility at varying of the building height in buildings with shear walls on the perimeter, two buildings, one mono-story and one 6-story, with shear walls at the ends are investigated.

2. Floor modeling

2.1. Description of the floor system

The floor system considered in this paper is composed of RC joists separated by lightening elements and a thin top RC slab, connecting the joists and the grid of the mutually perpendicular RC beams along the floor cell perimeter, shown in Fig. 1. A single floor cell is composed of a $4cm$ thick RC slab, eight $12cm \times 20cm$ (*width* $\times$ *height*) RC joists, nine strips of $48cm \times 20cm$ lightweight hollow bricks and four $30cm \times 52cm$ RC perimeter beams; see Fig. 2.

The beams, the slab and the joists are made of *C25/30* concrete, a very common grade in existing Italian buildings. The geometric and mechanical properties of the floor cell are shown in Table 1. The stiffness contribution of the hollow bricks was neglected on the basis of two considerations. The first one is the absence of connections between adjacent bricks of the same strip, which prevents both the transmission of traction and a reliable transmission of shear. The second one is related to brick brittleness, entailing that, when the floor is heavily loaded, the bricks break early, leaving to the RC elements alone the task of transmitting stresses.

2.2. The reference floor model (RM)

Following Pecce et al., the actual floor system is modeled through the software SAP2000 by means of solid FEs to represent each component. Since the slab behaves essentially as a membrane (plane stress state), a single element over the thickness suffices to describe its stress-strain field. The smallest dimension that drives the choice of the mesh size h is the slab thickness of $4cm$. For the slab in-plane discretization, a $6cm \times 6cm$ mesh is chosen. The mesh size is adapted in RC beams in order to get nodes belonging to the beams' main axis. Hence, to preserve the compatibility with internal floor cell solid elements, a $6cm \times 5cm \times 4cm$ mesh along the beams, and a $5cm \times 5cm \times 4cm$ mesh at beams intersection zones (see Fig. 3) are adopted.

In the 3D finite element model the properties of the lightening masonry elements were neglected for two reasons. One is that bond between lightening elements and the RC joists is weak compared to the bond between RC joists and the RC slab. As a consequence, when the

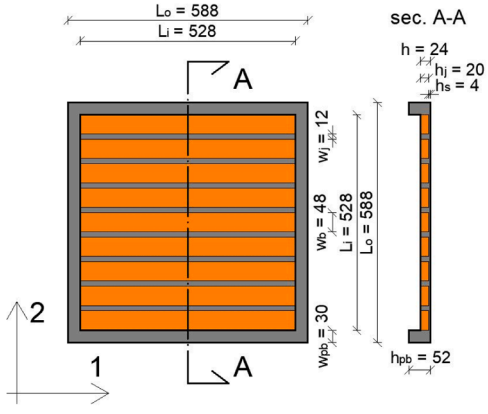

Fig. 2. Plan view and cross section of the RC floor cell made with standard ceiling bricks (dimensions are in centimeters) considered as case study.

Table 1
Geometric and mechanical properties of the floor.

L_o	5.88	m	Outside cell length
L_i	5.28	m	Inside cell length
L_m	5.58	m	Mean cell length
h_s	0.04	m	Slab thickness
h_j	0.20	m	Joist height
h	0.24	m	Floor height
w_j	0.12	m	Joist width
h_{pb}	0.52	m	Beam height
w_{pb}	0.12	m	Beam width
w_b	0.48	m	Brick width
A_c	0.422	m^2	Concrete Area of section A-A,Fig. 2
A_s	0.223	m^2	Slab transverse area
E_c	31476	MPa	Concrete Young's Modulus
G_c	13115	MPa	Concrete Shear Elastic Modulus
ν_c	0.20		Concrete Poisson's Ratio

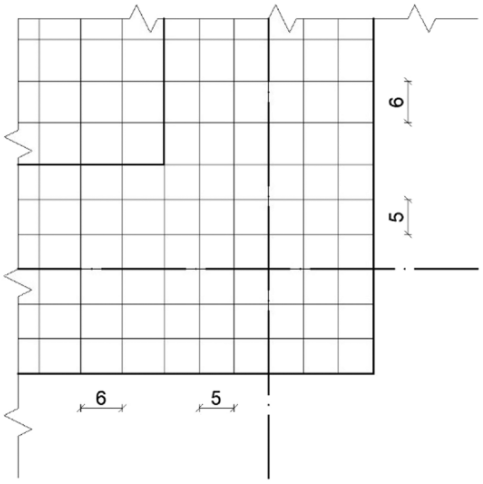

Fig. 3. Plan dimensions of the 3D mesh at floor cell corners.

floor cell undergoes to shear deformation, the bond between masonry elements and RC joist may not be enough to provide the shear transmission and a partial detachment of masonry elements may occur.

The other reason is that masonry elements contribute to floor in-plane stiffness when the floor cell undergoes to compression forces, however no contribution is given under tension. It follows that, when the floor is subject to seismic deformations masonry elements undergo to cracking.

For the reasons explained above, it cannot be relied on the stiffness contribution provided by the masonry elements. Moreover, neglecting the stiffness contribution of these elements subject to compression provides a lower bound estimate of the floor in-plane stiffness.

2.3. The simplified floor model (SM)

The simplified model of the floor cell is made by a flat orthotropic shell connected, along the perimeter, to 4 one-dimensional frame elements, representing the RC beams on the floor cell perimeter (Fig. 4). The floor cell dimensions are 558 cm x 558 cm, which coincide with the distances in the RM between two opposite beams. The shell element is coplanar with the grid formed by the frame elements.

The thickness assigned to the shell is equal to that of the RC slab in the RM, hence equal to 4 cm, to ease the results comparison between the SM and RM. An equivalent material density is assigned to the shell, to represent the entire floor weight. However, any value of shell thickness can be adopted, granted that the weight of the slab is maintained.

Beams' mechanical properties and geometric dimensions are the same of those assigned to the beams in the RM.

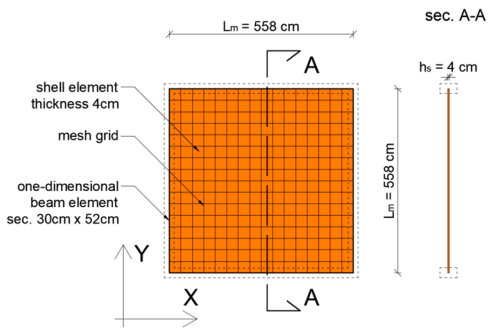

Fig. 4. Plan view and cross section of the SM floor cell with 16×16 mesh grid.

The mesh size was chosen according to a sensitivity analysis in which the mesh size was reduced until the floor displacement of the simplified model under in-plane compression loads had a maximum scatter of 1 % with respect to any fitter mesh. A discretization with 16×16 square finite elements is adopted. Consequently, the perimeter beams are divided into 16 frame elements, sharing their nodes with the shell element.

Since flat shells are able to carry both membrane and bending plate stresses, in order to promote a predominant membrane behavior, their bending stiffness is properly reduced, which also helps to prevent the formation of zero energy modes. To reproduce as best as possible the floor solid model behavior, the elastic properties of the orthotropic plate have to be calibrated, as shown in the following sections.

3. Homogenization

3.1. Basic homogenization procedures

Homogenization theories deal with heterogeneous media, bodies, or structures that may be considered as homogeneous at a large enough scale. With reference to Fig. 5, the basic assumption is the existence of a *Representative Volume Element* (*RVE*) with dimension l_{RVE}, able to represent any macroscopic portion of the body $\mathscr{B}$, such that

$$l_n \ll l_{RVE} \ll l, \tag{1}$$

where l is the characteristic length of $\mathscr{B}$, and l_n the characteristic length of the inhomogeneities.

There are two ways to determine the equivalent *RVE* material properties. One is the *kinematic approach*, which consists of applying a uniform strain kinematic boundary condition, i.e., a displacement field on the *RVE* boundary (∂RVE), of the type

$$\boldsymbol{u} = \boldsymbol{\varepsilon}_0 \boldsymbol{x} + \boldsymbol{\omega}_0 \boldsymbol{x} + \boldsymbol{c}_0 \qquad \forall \boldsymbol{x} \in \partial RVE \tag{2}$$

and to evaluate the corresponding mean stress field

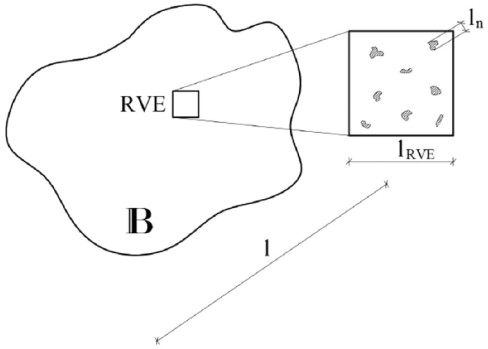

Fig. 5. Configuration of a macroscopically homogeneous body.

$$\langle \boldsymbol{\sigma} \rangle = \frac{\int_{RVE} \boldsymbol{\sigma} dV}{vol(RVE)}, \tag{3}$$

where $\boldsymbol{\varepsilon}_0$ is a constant symmetric tensor, $\boldsymbol{\omega}_0$ is a constant antisymmetric tensor, $\mathbf{c}_0$ is a constant vector, and $\boldsymbol{\sigma}$ is the Cauchy stress tensor. It should be noted that $\boldsymbol{\omega}_0$ and $\mathbf{c}_0$ are responsible for a pure rigid motion of the RVE. Furthermore, it can be easily shown that the mean strain $\langle \boldsymbol{\epsilon} \rangle$ of the RVE coincides with $\boldsymbol{\epsilon}_0$ (by using Eq. (9)). Then, the homogenized elastic tensor $\langle \mathbf{C} \rangle$ is defined as the four-order tensor such that

$$\langle \boldsymbol{\sigma} \rangle = \langle \mathbb{C} \rangle \langle \boldsymbol{\epsilon} \rangle \tag{4}$$

for any choice of the symmetric tensor $\boldsymbol{\epsilon}_0$, i.e., for any choice of $\langle \boldsymbol{\epsilon} \rangle$.

Assuming that the RVE possesses orthotropic symmetries with respect to the Cartesian coordinates x_1, x_2 and x_3, using Voigt notation and omitting the surrounding angular brackets on symbols Eq. (4) becomes

$$\begin{bmatrix} \sigma_{11} \\ \sigma_{22} \\ \sigma_{33} \\ \sigma_{12} \\ \sigma_{13} \\ \sigma_{23} \end{bmatrix} = \begin{bmatrix} C_{11} & C_{12} & C_{13} & 0 & 0 & 0 \\ & C_{22} & C_{23} & 0 & 0 & 0 \\ & & C_{33} & 0 & 0 & 0 \\ & & & C_{44} & 0 & 0 \\ & \text{Sym.} & & & C_{55} & 0 \\ & & & & & C_{66} \end{bmatrix} \begin{bmatrix} \varepsilon_{11} \\ \varepsilon_{22} \\ \varepsilon_{33} \\ 2\varepsilon_{12} \\ 2\varepsilon_{13} \\ 2\varepsilon_{23} \end{bmatrix} \tag{5}$$

Focusing on plane stress only, it is

$$\begin{bmatrix} \sigma_{11} \\ \sigma_{22} \\ \sigma_{12} \end{bmatrix} = \begin{bmatrix} C_{11} & C_{12} & 0 \\ & C_{22} & 0 \\ Sym. & & C_{44} \end{bmatrix} \begin{bmatrix} \varepsilon_{11} \\ \varepsilon_{22} \\ 2\varepsilon_{12} \end{bmatrix} \tag{6}$$

where the elasticity parameters C_{ij} are related to the four engineering constants E_1, E_2, G_{12} and ν_{12} by

$$\begin{aligned} C_{11} &= \frac{E_1}{1-\nu_{12}\nu_{21}}, \\ C_{22} &= \frac{E_2}{1-\nu_{12}\nu_{21}}, \\ C_{12} &= \nu_{21} C_{11} = \nu_{12} C_{22}, \\ C_{44} &= G_{12}, \\ E_1 \nu_{21} &= E_2 \nu_{12}. \end{aligned} \tag{7}$$

By using three different and linear independent $\boldsymbol{\epsilon}_0$ in the boundary conditions (2) and recalling that $\langle \boldsymbol{\varepsilon} \rangle = \boldsymbol{\epsilon}_0$, one gets the four elastic parameters in (6) and thus, by inverting (7), the four engineering constants.

The other way to determine the equivalent *RVE* material properties is the *static approach*, which consists of applying the homogeneous mechanical boundary condition

$$\boldsymbol{t} = \boldsymbol{\sigma}_0 \boldsymbol{n} \quad \text{on } \partial\text{RVE} \tag{8}$$

where $\boldsymbol{\sigma}_0$ is a constant symmetric tensor and $\mathbf{n}$ is the boundary outer normal vector, and then evaluating the corresponding mean strain $\langle \boldsymbol{\varepsilon} \rangle$. Since it can be shown that $\langle \boldsymbol{\sigma} \rangle = \boldsymbol{\sigma}_0$, by varying $\boldsymbol{\sigma}_0$ from Eq. (6) one gets again the four elastic parameters C_{ij}. It is worth noting that the mean strain depends only on the boundary displacements $\mathbf{u}$, since, by using the Gauss-Green integration theorem, it is

$$\int_{RVE} \epsilon_{ij} dV = \frac{1}{2} \int_{\partial RVE} u_i n_j + u_j n_i dA. \tag{9}$$

When $l_n << l_{RVE}$ the coefficients determined by the two procedures are very close and coincide at the limit $\frac{l_n}{L_{RVE}} \to 0$.

Both approaches require the solution of an elastic equilibrium problem with different boundary conditions. Since exact analytical solutions of the equilibrium problem are not generally available, many approximate methods to estimate the equivalent parameters were proposed.

Among them, Voigt bounds (iso-strain model) are obtained by assuming, in the kinematic approach, a uniform strain field [42] in the place of the true solution, i.e., taking $\boldsymbol{\varepsilon}(\mathbf{x}) = \boldsymbol{\varepsilon}_0$ for all $\mathbf{x} \in \mathscr{B}$. So doing, the mean stress field can be explicitly evaluated by

$$vol(\mathscr{B}) \langle \boldsymbol{\sigma} \rangle = \int_{\mathscr{B}} \mathbb{C}(\boldsymbol{x}) \boldsymbol{\varepsilon}_0 dV = \int_{\mathscr{B}} \mathbb{C}(\boldsymbol{x}) dV \boldsymbol{\varepsilon}_0 \tag{10}$$

and thus, by (4)

$$\langle \mathbb{C} \rangle^{Voigt} = \frac{\int_{\mathscr{B}} \mathbb{C}(\boldsymbol{x}) dV}{vol(\mathscr{B})}. \tag{11}$$

For a heterogeneous body made by N homogeneous materials (phases), the above equations transform in the well-known *rule of mixtures*

$$\langle \mathbb{C} \rangle = \sum_{i=1}^{N} \mu_i \mathbb{C}_i, \tag{12}$$

where μ_i and $\mathbb{C}_i$ are the volume (area) fraction and the elastic tensor, respectively, of phase *i*.

For a fiber reinforced lamina, the rule of mixtures provides good estimates of the longitudinal (aligned with fibers) elastic modulus (see Ch. 3 in [42])

$$\langle E_1 \rangle = \mu_m E_m + \mu_f E_f \tag{13}$$

where μ_m and E_m are the matrix volume fraction and the matrix elastic modulus, respectively, while μ_f and E_f are the analogous parameters for the fibers. The rule of mixtures performs well also for the prediction of the main Poisson's ratio.

$$\langle \nu_{12} \rangle = \mu_m \nu_m + \mu_f \nu_f. \tag{14}$$

Conversely, Reuss bounds (iso-stress model) are obtained by assuming a constant stress field within the static homogenization approach and, when applied to a fiber reinforced lamina, provide rough estimates for the transverse elastic modulus

$$\langle E_2 \rangle^{-1} = \mu_m E_m^{-1} + \mu_f E_f^{-1} \tag{15}$$

and for the shear elastic modulus

$$\langle G \rangle^{-1} = \mu_m G_m^{-1} + \mu_f G_f^{-1}. \tag{16}$$

The latter two formulas are also known as the *inverse rule of mixtures*.

To apply the homogenization procedures to the floor system, a floor cell is assumed as the RVE, being well aware, however, that neither of the hypothesis in (1) are satisfied rigorously. As a matter of fact, the dimensions of inhomogeneities (e.g., the joist spacing) are comparable to that of the cell, violating the condition $l_n \ll l_{RVE}$ and preventing a clear and unique definition of the *RVE* properties. Consequently, the kinematic and the static approaches may provide quite different estimates of the equivalent elastic parameters.

Moreover, since a typical floor system is usually composed of a finite and small number of floor cells, arranged along a few rows and columns, with sizes comparable to that of the floor, the condition $l_{RVE} << l$ is also violated. Consequently, the equivalent cell properties may not adequately represent those of the whole floor. With all these uncertainties, the choice of the equivalent properties must necessarily be guided by numerical comparison.

It is worth noting that, although the only part of the floor cell that needs to be homogenized is the internal one, comprising the slab, joist and lightening elements, it is not possible to analyze the internal part and the surrounding frames separately, neither in the solid model nor in the simplified model. In doing so, displacement compatibility between the two parts would be lost. Only in the case of the kinematic approach applied to the simplified model, is separation possible, because compatibility is forced by the kinematic boundary condition.

3.2. Analytical estimates of equivalent properties (ANH)

Simple estimates of the equivalent orthotropic slab moduli E_1, E_2, ν_{12} and G can be obtained by formulas widely employed in the field of fiber reinforced composite micro mechanics, based on the iso-stress and iso-strain models.

To this aim, the internal part of the floor solid cell is regarded as a composite laminate of thickness $h = h_s + h_j$ and plane dimensions $L_i \times L_i$ made by two laminae: the first one homogeneous, with thickness h_s, which represents the concrete slab; the second one of thickness h_j, made by the joists, with a total section area $A_j = 8h_j w_j$. Both laminae and the bricks are aligned with direction 1, in Fig. 6.

To evaluate the equivalent stiffness parameters E_1 and ν_{12} by the kinematic homogenization procedure, a unitary displacement is applied along the *axis 1*. Then, by the iso-strain assumption the following estimates of the resultant forces are obtained on two orthogonal sections of the solid model.

$$\begin{aligned} F^1_{3D} &= (A_s + A_j) \times E_c, \\ F^2_{3D} &= (A_s + A_j) \times E_c \times \nu_c, \end{aligned} \tag{17}$$

Then, the same boundary displacement applied to the solid cell is applied to the internal part of the simplified floor cell made by a homogeneous and orthotropic lamina with in-plane sizes $L_m \times L_m$ and thickness h_s. The resultant forces on two orthogonal sections are evaluated exactly as

$$\begin{aligned} F^1_{2D} &= A_s \times \frac{E_1}{1 - \nu_{12}\nu_{21}}, \\ F^2_{2D} &= A_s \times \frac{E_1}{1 - \nu_{12}\nu_{21}}\nu_{12}. \end{aligned} \tag{18}$$

Imposing the equality between the resultant forces of the two models, the following two equations

$$\begin{aligned} A_s \times \frac{E_1}{1 - \nu_{12}\nu_{21}} &= (A_s + A_j) \times E_c, \\ A_s \times \frac{E_1}{1 - \nu_{12}\nu_{21}}\nu_{12} &= (A_s + A_j) \times E_c \times \nu_{12}, \end{aligned} \tag{19}$$

with three unknown parameters E_1, ν_{12}, ν_{21} are derived.

To get a third equation involving explicitly E_2, the static approach is used. A unitary uniform boundary stress distribution is applied in direction 2 (orthogonal to the joist direction). Neglecting the joist contributions, as the stress spreads very little in them, one gets

$$E_2 = E_c, \tag{20}$$

which, along with Eqs. (18) and (7−5), determines $E_1, E_2, \nu_{12}, \nu_{21}$ uniquely.

The evaluation of the equivalent shear modulus G is more complicated. Since the shear modulus of the bricks is assumed to be zero, the iso-stress formula (16) predicts a vanishing shear modulus for the joist-brick lamina. Thus, only the slab lamina contributes, and the equivalent laminate shear modulus would be

$$G = G_c. \tag{21}$$

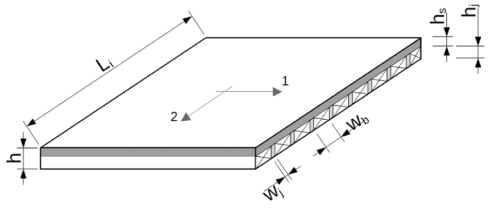

Fig. 6. Internal part of the floor cell regarded as a composite laminate made by two plies, the homogeneous RC slab and the joist-brick lamina.

This expression definitely underestimates the floor shear stiffness, because it does not consider the joists' collaboration with the slab.

On the other hand, ignoring the bricks, and treating the floor as a one directional ribbed plate, the iso-strain approach would predict an exaggerated and unrealistic large shear modulus

$$G = \frac{A_s + A_j}{A_s} G_c \tag{22}$$

because it assumes the whole joists section A_j to be in a uniform shear strain-stress state, whereas, in reality, stress spreads on a small portion of the joists. A reasonable estimate can be obtained by assuming the collaborating joist portion to be a triangle with sides inclined by 45° to the slab, with area

$$a^*_j = w_j \times w_j \big/ 4, \tag{23}$$

resulting in the estimated shear modulus

$$G = \frac{A_s + \alpha A_j}{A_s} G_c \tag{24}$$

where $\alpha = \frac{w_j}{4h_j}$.

To verify the plausibility of this assumption, a FE analysis on a solid portion of the floor including one joist and its adjacent slab (Fig. 7), loaded by the uniform boundary shear stress $\tau_b = 1MPa$, is performed. Two different joists widths of $6cm$ and $14cm$ are considered. The results are shown in Fig. 8, where the shear stress color map is presented. The map confirms that shear spreads into the joist roughly in the supposed triangular region, but with much lowered values, in the range $0.1\tau_b \div 0.4\tau_b$.

Also, the perimeter RC beams give a contribution, similar to that of the joists, to the floor shear stiffness. Since the assessment is performed on a single floor cell, only a half-perimeter beam cross section need be considered, so that at each end, the beam contribution to the shear area is assumed to be

$$A^*_{pm} = (w_{pb}/2) \times (w_{pb}/2) \big/ 2 \tag{25}$$

Thus, the formula for the equivalent shear stiffness turns to be

$$G = \frac{A_s + \frac{w_j}{4h_j} A_j + \frac{w^2_{pb}}{4}}{A_s} G_c. \tag{26}$$

Numerical values evaluated by Eqs. (18) – (19) – (20) – (26) for data in Table 1 are given in the second row (ANH) of Table 2.

3.3. Standard static homogenization (SSH)

The purpose is to determine the properties of the equivalent simplified model by requiring that its mean strain response be equal to that of the reference model when the models are loaded with the same homogeneous boundary loads. To calculate the mean strain, formula (9) is used, which turns to be

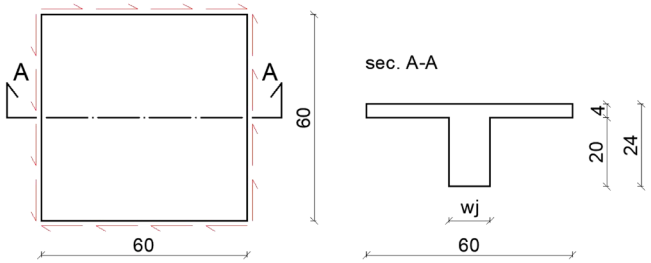

Fig. 7. Geometric configuration of the model (dimensions in centimeters).

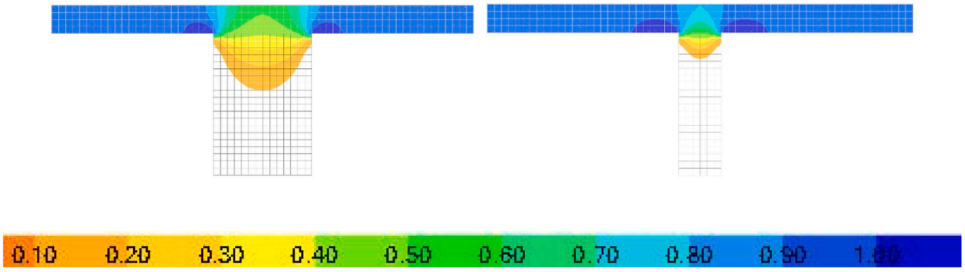

Fig. 8. Shear stress maps in the floor cross section loaded by uniform boundary shear. Only shear stress between 0.1 MPa (light orange) and 1.1 MPa (dark blue) are shown.

Table 2
Elastic constants for the equivalent orthotropic plate obtained from three different homogenization techniques. RC slab constants are reported for the sake of comparison.

	E_1 [GPa]	E_2 [GPa]	ν_{12}	ν_{21}	G [GPa]
RC Slab	31.5	31.5	0.20	0.20	13.1
ANH	54.6	31.5	0.20	0.16	15.4
SSH	70.0	37.5	0.14	0.09	14.9
LFH	26.5	21.3	0.20	0.16	14.6

$$\bar{\epsilon}^{RM}_{\alpha\beta} = \frac{1}{2|A_{RM}|}\int_{\partial RM} u_\alpha n_\beta + u_\beta n_\alpha dA \tag{27}$$

for the reference model, and

$$\tilde{\epsilon}^{SM}_{\alpha\beta} = \frac{1}{2|L_{SM}|}\int_{\partial SM} u_\alpha n_\beta + u_\beta n_\alpha dL \tag{28}$$

for the simplified model, with $\alpha, \beta \in \{1,2\}$. In Eqs. (27) and (28) $|A_{RM}|$ and $|L_{SM}|$ indicate the area and the length of the integration domain, respectively. It is worth noting that while (27) rigorously expresses the solid floor cell mean strain, at least for the in-plane components, Eq. (28) expresses the mean strain on the equivalent plate alone, without the contribution of the surrounding frame elements. For this reason, the mean strain is marked by tilde symbol in place of the bar.

A floor solid cell loaded by three different boundary forces of the type (8) characterized by different choices of $\boldsymbol{\sigma}_0$, as shown in Fig. 9, are considered.

Load condition 1: longitudinal compression. Choosing $\sigma_{011} = -p$ as the only non vanishing component of $\boldsymbol{\sigma}_0$, the boundary forces reduce to a uniform horizontal pressure on the outer faces of beams $A-D$ and $B-C$ (Fig. 9-a). To suppress rigid motions, the mid-node of beams AD is restrained in both in-plane directions; the mid-node of beams BC is restrained only in the 2-direction, while all the slab top nodes are restrained in the direction normal to the plane. The value of p is chosen so that the resultant compression force equals $1000kN$.

Load condition 2: transverse compression. The only non-vanishing component of $\boldsymbol{\sigma}_0$ is $\sigma_{022} = -p$, so that the boundary forces reduce to a compressive distribution applied to beams AB and DC; see Fig. 9-b. The mid-node of beam AB is restrained along both in-plane directions; the mid-node of beam CD is restrained along the 1-direction, while the slab top nodes are restrained in the direction normal to the plane.

Load condition 3: plane shear. The non vanishing components of $\boldsymbol{\sigma}_0$ are $\sigma_{012} = \sigma_{021} = \tau$, and the boundary force distribution induce pure shear strains, as shown in Fig. 9-c. τ is chosen so that the resultant shear force on each cell side is $1000\sqrt{2}kN$. Rigid motions are prevented, restraining the translation of node A in both in-plane directions, fixing node D along the 1-direction and restraining the slab top nodes along the direction normal to the plane.

For each load case the nodes' displacements are obtained by the FE analysis. Since the mean strain is evaluated by (27) only, the lateral boundary displacements are needed. The displacements of the reference model have to be compared with those of the simplified model whose boundary sides coincide with the axes of the beams in the reference model. Consequently, for this model, the displacements of the nodes lying on the vertical planes passing through the beams' axes are considered (Fig. 10).

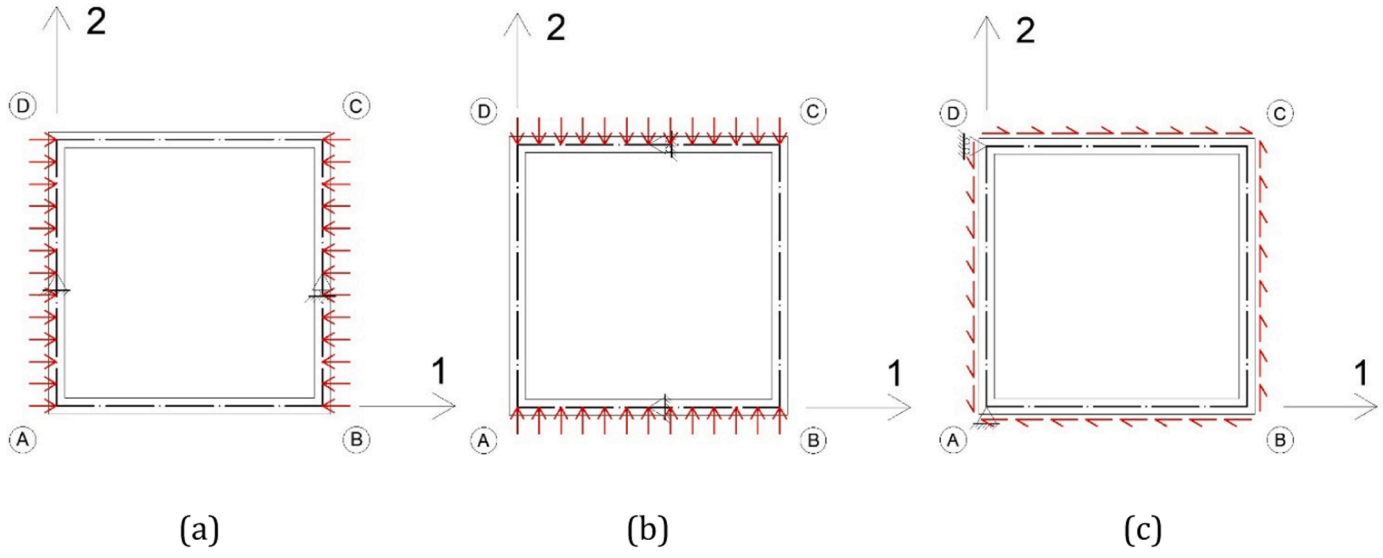

Fig. 9. SSH load cases.

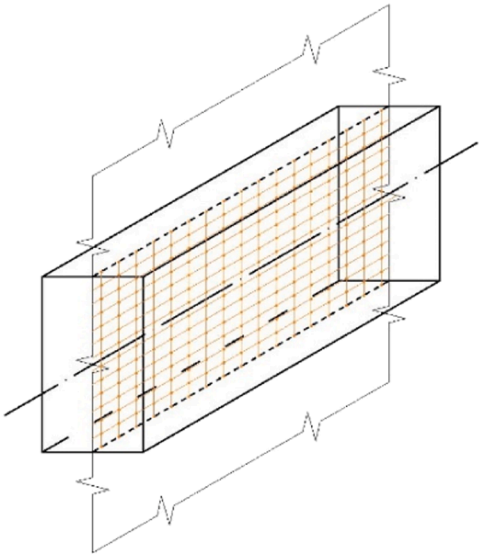

Fig. 10. Beam nodes belonging to the vertical plane passing through beam's axis in the solid elements model.

Thus, for the reference model (27),

$$\begin{aligned}\bar{\epsilon}_{11}^{RM} &= \frac{1}{L_i}\left(u_1^{BC} - u_1^{AD}\right),\\ \bar{\epsilon}_{22}^{RM} &= \frac{1}{L_i}\left(u_2^{DC} - u_2^{AB}\right),\\ \bar{\epsilon}_{12}^{RM} &= \frac{1}{2L_i}\left(u_2^{BC} - u_2^{AD} + u_1^{DC} - u_1^{AB}\right),\end{aligned} \tag{29}$$

where u_α^{XY} is the average displacement in α direction on the vertical plane passing through nodes X and Y. The same relation holds also for the simplified model, considering the mean side displacements on the boundary lines. Since $\bar{\epsilon}_{\alpha\beta}^{RM}$ are known from the FE analysis, the elastic constant $\boldsymbol{\xi} = (E_1, E_2, \nu_{12}, G)$ of the simplified model should satisfy the following three implicit numerical equations

$$\tilde{\epsilon}_{\alpha\beta}^{SM}(\boldsymbol{\xi}) - \bar{\epsilon}_{\alpha\beta}^{RM} = 0, \qquad \alpha,\beta = 1,2, \tag{30}$$

for each of the three independent load cases. This is a classical fitting problem with nine implicit equations and only four unknowns that can be solved by least square techniques, e.g., by minimizing the error function

$$\chi^2(\boldsymbol{\xi}) = \sum\nolimits_{\alpha,\beta,n}\left(\tilde{\epsilon}_{\alpha\beta,n}^{SM}(\boldsymbol{\xi}) - \bar{\epsilon}_{\alpha\beta}^{RM}(n)\right)^2 \tag{31}$$

where $n = 1,\ 2,\ 3$ is the load case index. It is highlighted that any error function evaluation requires the solution of a 2D FE model with three load cases. Furthermore, an integration between the least square algorithm and the FE package is required.

A simplified partial optimization procedure can be conceived, if the response to one load case is governed by material parameters that are different from the other two load cases. Since the inverted constitutive equations for the orthotropic plate, in terms of mean values, are

$$\begin{aligned}\langle\epsilon_{11}\rangle &= \frac{1}{E_1}\left(\langle\sigma_{11}\rangle - \nu_{12}\langle\sigma_{22}\rangle\right),\\ \langle\epsilon_{22}\rangle &= \frac{1}{E_2}\left(\langle\sigma_{22}\rangle - \nu_{21}\langle\sigma_{11}\rangle\right),\\ \langle\epsilon_{12}\rangle &= \frac{1}{2G}\langle\sigma_{12}\rangle.\end{aligned} \tag{32}$$

In the absence of the beam elements surrounding the orthotropic plate, for load case 1 the value $\langle\sigma_{22}\rangle$ would vanish and $\langle\epsilon_{11}\rangle$ would depend only on E_1. Actually, the presence of the beam elements alters the stress distribution and, although the mean of σ_{22} still vanishes on the whole simplified element, it does not necessarily vanish on the plate alone. However, if it still remained small, $\langle\epsilon_{11}\rangle$ would depend very little on ν_{12}, E_2 and G. To verify this guess, a numerical sensitivity analysis aimed to assess the effects of material parameters' variations on $\tilde{\epsilon}_{11,1}^{SM}(\boldsymbol{\xi})$ was performed. It turned out that, while a 1% variation of E_1 produces a $0.35 \div 0.71\%$ change on $\tilde{\epsilon}_{11,1}^{SM}(\boldsymbol{\xi})$, a 1% variation of the other parameters produces a $10 \div 20$ times smaller change ($0.05 \div 0.1\%$) in the range of material parameters for the whole simplified element.

Similarly, it was verified that $\tilde{\epsilon}_{22,2}^{SM}(\boldsymbol{\xi})$ strongly depends on E_2 and much less on the other parameters, while $\tilde{\epsilon}_{12,3}^{SM}(\boldsymbol{\xi})$ depends almost exclusively on G.

Taking on this insight, an algorithm to estimate the material parameters is proposed, leaving the results verification to numerical comparison. *The algorithm:*

1. A starting set $\boldsymbol{\xi}^{(0)}$ of the material properties is chosen according to the first row of Table 2, corresponding to the assumption that the equivalent plate behaves as the homogeneous concrete slab.
2. Using an appropriate algorithm, the following problems are solved consecutively
   a. Find $E_1^{(1)}$ such that
   $$f_1\left(E_1^{(1)}\right) = \left|\tilde{\epsilon}_{11,1}^{SM}\left(E_1^{(1)}, E_2^{(0)}, \nu_{12}^{(0)}, G^{(0)}\right) - \tilde{\epsilon}_{11,1}^{RM}\right| < toll\cdot\tilde{\epsilon}_{11,1}^{RM} \tag{33}$$
   b. Find $E_2^{(1)}$ s.t.
   $$f_2\left(E_2^{(1)}\right) = \left|\tilde{\epsilon}_{22,2}^{SM}\left(E_1^{(1)}, E_2^{(1)}, \nu_{12}^{(0)}, G^{(0)}\right) - \tilde{\epsilon}_{22,2}^{RM}\right| < toll\cdot\tilde{\epsilon}_{22,2}^{RM} \tag{34}$$
   c. Find $G^{(1)}$ s.t.
   $$f_3\left(G^{(1)}\right) = \left|\tilde{\epsilon}_{12,3}^{SM}\left(E_1^{(1)}, E_2^{(1)}, \nu_{12}^{(0)}, G^{(1)}\right) - \tilde{\epsilon}_{12,3}^{RM}\right| < toll\cdot\tilde{\epsilon}_{12,3}^{RM} \tag{35}$$
   d. Find $\nu_{12}^{(1)}$ s.t.
   $$f_4\left(\nu_{12}^{(1)}\right) = \left|\tilde{\epsilon}_{22,1}^{SM}\left(E_1^{(1)}, E_2^{(1)}, \nu_{12}^{(1)}, G^{(1)}\right) - \tilde{\epsilon}_{22,1}^{RM}\right| < toll\cdot\tilde{\epsilon}_{22,1}^{RM} \tag{36}$$
3. Steps 2-5 are repeated until the parameters stabilize, that is until
   $$\left|\frac{\xi_i^{(n)} - \xi_i^{(n-1)}}{\xi_i^{(n)}}\right| < toll \quad \forall\, i = 1,2,3,4. \tag{37}$$

In applying the algorithm to the considered case study, it turned out that at the second cycle (a cycle is made by steps 2–5) the maximum variation in parameters was about 1%, while in the third cycle the variations were negligible. Thus, a single cycle could be enough to determine a sufficiently accurate estimate of the elastic constants of the equivalent orthotropic plate. Numerical estimates are collected in the third row of Table 2.

As for the solution of steps (a)-(c), any nonlinear root finding algorithm can be applied (e.g. bisection, Newton, secant…). For instance, for the problem in step (a) consisting of finding the root $x = E_1^{(1)}$ of the implicit function

$$f_1(x) = \tilde{\epsilon}_{11,1}^{SM}\left(x, E_2^{(0)}, \nu_{12}^{(0)}, G^{(0)}\right) - \tilde{\epsilon}_{11,1}^{RM}. \tag{38}$$

A single step of the secant method would consist of solving the linear

equation

$$f_1(x_1)+\frac{f_1(x_2)-f_1(x_1)}{x_2-x_1}x=0, \tag{39}$$

where x_1, x_2 are the last two estimates of E_1. However, since $\widetilde{\epsilon}^{SM}_{11,1}$ is expected to be nearly proportional to $(E_1)^{-1}$; that is

$$f_1(E_1)\approx\alpha+\frac{\beta}{E_1} \tag{40}$$

for suitable constants α, β, Eq. (35) is replaced by

$$f_1(x_1)+\frac{f_1(x_2)-f_1(x_1)}{\frac{1}{x_2}-\frac{1}{x_1}}\left(\frac{1}{x_1}-\frac{1}{x}\right)=0, \tag{41}$$

to obtain a much faster convergence. Two iterations were sufficient to get a root with *toll* $< 1\%$, while many more were needed for the standard bisection.

3.4. Homogenization through lumped forces (LFH)

Although the standard static homogenization procedure relies on strong mathematical foundations, since the underlying hypotheses are not fully satisfied by the floor cell, it is not expected to produce optimal results. Furthermore, the SSH procedure is based on the response of the floor cell to distributed forces on its boundary, while in reality, especially in multi-story buildings, external forces are mainly exerted by the vertical elements, i.e., by columns or shear walls, at the cell corner nodes, as made in [43]. This observation suggests considering a homogenization procedure based on the response of the cell to forces lumped at the corner nodes. The three considered load cases are illustrated in Fig. 11.

These load cases mimic the corresponding ones defined in SSH: compression of the floor cell along directions 1, 2 and in-plane shear, respectively. Out of plane displacements at all the floor top nodes are restrained, while the restraints applied to the in-plane displacements are shown in Fig. 11.

Since a corner node in the simplified model corresponds to a solid prismatic region of the solid model (corner region, Fig. 12), a corner force in the solid model is divided equally among all mesh nodes forming the corner region. For the same reason the corner displacement of the solid model is defined as the mean displacement of all nodes in the corner region.

The mean strains of the reference and simplified models are taken again according to Eq. (29), but the mid-side displacements are evaluated as the mean of the corresponding displacements of the two adjacent

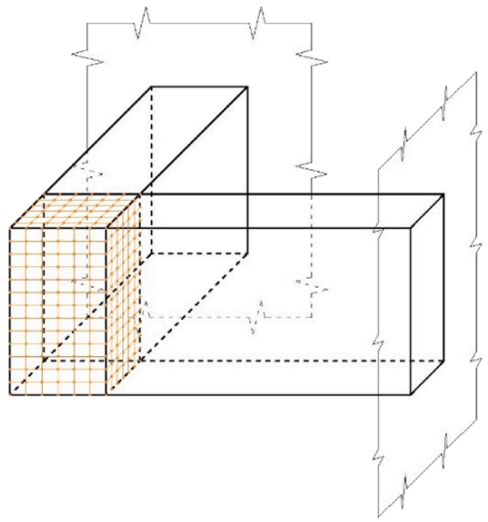

Fig. 12. A corner region of the solid FE model made by the solid intersection of two RC beams.

corner nodes; that is, for instance

$$u_1^{BC}=\frac{u_1^B+u_1^C}{2}, \tag{42}$$

The equivalent plate elastic constants are again evaluated by solving Eq. (30), by means of the algorithm proposed in Section 3.3 for SSH technique. The results are reported in the fourth row of Table 2.

3.5. Homogenization results comparison

With reference to Table 2, it is noted that the ANH estimates of the elastic constants are intermediate, between those achieved by SSH and LFH, with the only exception of the shear modulus G, which, however, is very similar in all the three procedures. Hence, the ANH procedure turns out to be a good candidate for the determination of the equivalent characteristics, because it does not require the development of floor FE models. It is also noted that, between the two numerical procedures, LFH provides values of the elastic moduli E_1, E_2 and G smaller than those provided by SSH. This difference is due to the fact that, when the in-plane compression is applied according to SSH, the external forces are uniformly applied along the floor cell side. Hence, they spread mainly into the shell element, while only a lower amount spread into the perimeter beams. The deformation of the floor cell side is computed as

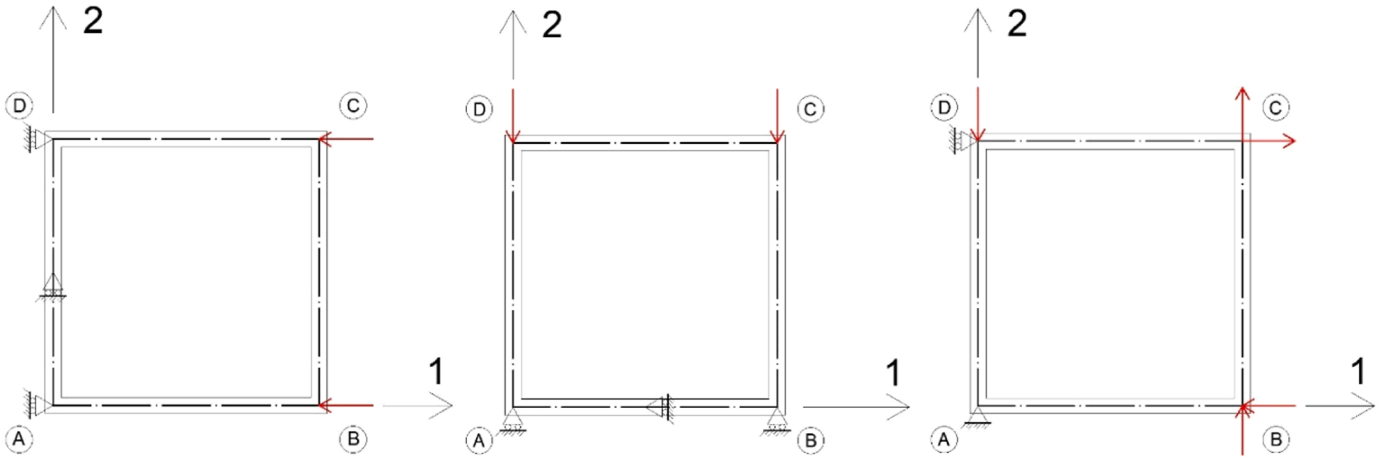

Fig. 11. LFH load cases.

the average deformation of the floor cell side, which is mainly determined by the displacements of the shell element, and, hence, by the shell stiffness.

Conversely, when the in-plane compression is applied according to LFH, the external forces are lumped at beams' joints [44,45]. Hence, they spread mainly into perimeter beams, while only a lower amount into the nearby portion of the shell. In this case the deformation of the floor cell is computed as the average value of the displacements of the beams' nodes, which is mainly determined by beams' axial stiffness.

Since the beams' axial stiffness is much greater than that of the shell element, from the above it follws that applying the same resultant force in SSH and LFH leads to estimates of the shell elastic constants E_1 and E_2 that are lower in LFH.

Moreover, it worth noting that LFH is the only approach that returns values of elastic moduli E_1 and E_2 smaller than the concrete modulus E_c. This outcome seems paradoxical but can be explained by the fact that the loads concentrated at the perimeter beams' end nodes spread more in the beams, due to their high axial stiffness, and less into the internal part of cell. Consequently, the stiffness contribution of the internal part is secondary with respect to that of the beams.

From the fifth column of Table 2 it is also observed that the shear modulus G given by the three methods is always higher (by at least 10 %) than that of the RC slab. It follows that all the proposed methods are able to capture joists' contribution to the shear stiffness of the floor cell.

4. Performance evaluation of homogenized models

4.1. One-story structures

According to [13], the effects of floor slab flexibility are amplified in buildings with a large in-plane aspect ratio and shear walls along the short sides of the floor. For this reason, two one-story structures with these features are analyzed. In the first one, the floor is composed of four aligned cells (1 × 4 floor) supported by shear walls along the short sides and columns along the long sides (Fig. 13). The floor aspect ratio is 4 : 1; i.e., the maximum value for which Eurocode 8 allows the rigid diaphragm assumption. In the second structure, the floor is composed by eight floor cells arranged along two rows (2 × 4 floor system) with 2 : 1 aspect ratio (Fig. 14). A uniformly distributed horizontal load parallel to Y-direction is applied to the floor's bearing beams, considering both floor joist orientations, as in Fig. 15 and Fig. 16.

The models of the structures are then analyzed, assigning each time one of the four different sets of the elastic constants reported in the rows of Table 2. Two more models for each structure are analyzed, where in the former the floor is modeled by solid elements, while in the latter by adopting the rigid diaphragm hypothesis. In all models the columns and the shear walls are modeled using one-dimensional frame elements endowed with shear flexibility.

The results of the analyses are shown in terms of normalized horizontal displacement $u = \frac{U}{U^{ref}}$ and normalized base shear $v = \frac{V}{V^{ref}}$ at nodes A and C (Fig. 13 and Fig. 14). These two nodes were selected, because the former is subjected to the smaller displacements and the latter to the greater ones in the cases where the floor is flexible. The reference values

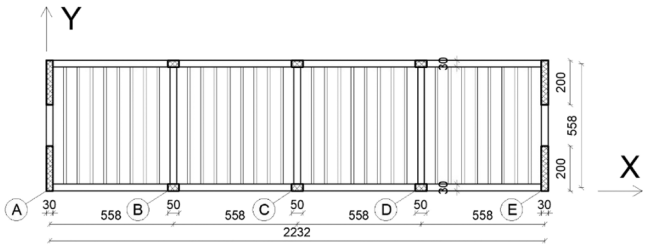

Fig. 13. Plan of the structure with 1 × 4 floor systems.

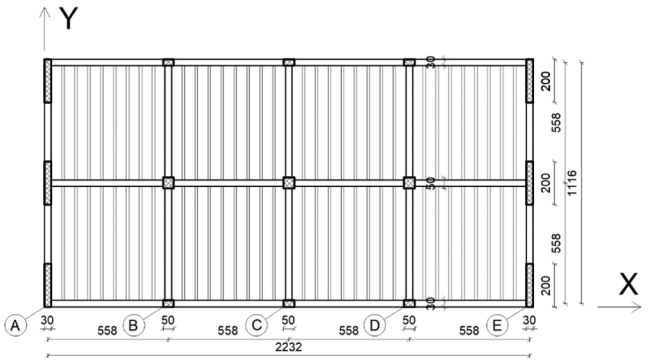

Fig. 14. Plan of the structure with 2 × 4 floor systems.

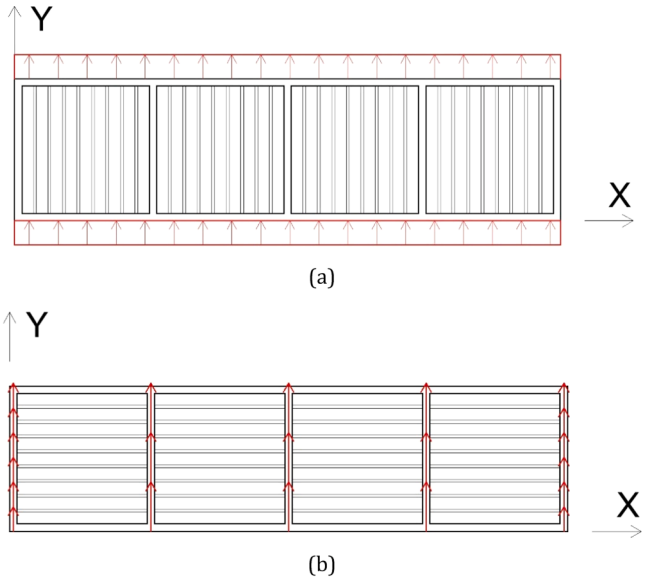

Fig. 15. One-story 1 × 4 structures, with joists (a) parallel to and (b) orthogonal to the loading direction.

of node displacements, U^{ref}, and column or wall shears, V^{ref}, are those obtained for the structures where floors are modeled by solid FEs. Furthermore, in-plane normalized drifts, $\Delta = \frac{U_C - U_A}{U_A}$, are computed to quantify the floor in-plane deformation.

The numerical results are reported in Tables 3 and 4, whereas Fig. 17 renders graphically the in-plane relative drifts Δ and the relative base shears, computed as the ratios between the base shears at nodes A, B, C, D, E and their sum, respectively.

The first important outcome that can be derived from the results reported in Tables 3 and 4 and Fig. 17 is that, in all cases, both the nodal displacements and the base shears predicted by the three homogenization methods are very similar to each other and close to the reference values. The maximum error in the displacements with respect to the reference model is 8.6% at node A of the SSH model with the joists oriented along the Y-direction, and the maximum error in base shears is 5.9% at node C of the SSH model with the joists oriented along the X-direction. It turns out that the analytical method is able to give results in term of floor displacements and base shear as good as those obtained by the other procedures (SSH and LFH). However, this method requires lower computational cost, hence its use is more convenient and faster.

The second important result is the total inadequacy of the rigid diaphragm assumption, since it predicts a base column shear at node C that is less than one-fifth of the reference shear in the 1 × 4 structure and about one-third of that in the 2 × 4 case. While the 1 × 4 structure is a

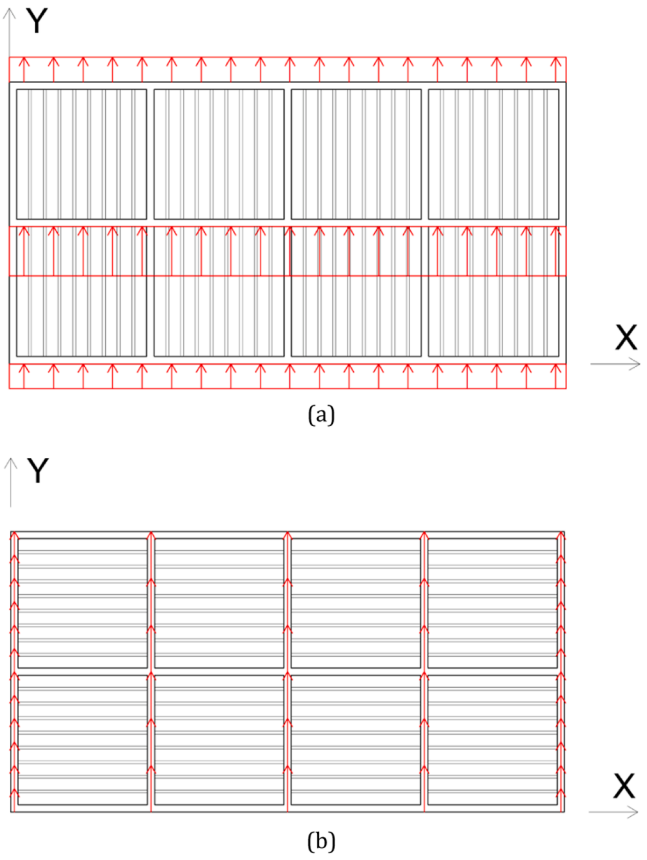

Fig. 16. One-story 2 × 4 structures, with joists (a) parallel to and (b) orthogonal to the loading direction.

rather extreme case, the 2 × 4 is not.

It is also important to note that, for the considered case studies, modeling the in-plane floor flexibility taking into account only the floor RC slab leads to good results both in terms of relative drifts and base shears. Actually, the largest errors on Δ and v_C are 13.0% and 6.1%, respectively, for the 2 × 4 structure model with joists oriented along the X-direction. In view of these low error values, which are only a few percentage points larger than those of the other models, from the computational point of view, the use of the equivalent slab is a convenient alternative to these models.

4.2. Multi-story structures

The use of shear walls is much more common in structures made of several stories. Considering the same two floor systems and the same structural plan configurations of the one-story structures, two six-story buildings are analyzed. Two different vertical load patterns are considered, both consisting of uniform distributions of horizontal forces applied at floor levels similarly to those applied to the one-story structures. A "modal" and a "uniform" lateral load pattern are adopted to represent the lateral load distribution into the undamaged structure and into the fully damaged structure, respectively. In the "modal" load pattern the forces are linearly increasing with the building height, as it occurs in the modal load distribution of a regular building. In the "uniform" load pattern the forces have the same magnitude at all floors (constant load), since the floor mass is equal for all floors.

Focusing on the first story, it should be noticed that most of the horizontal forces acting on the floor are transferred by the upper vertical elements, columns or walls, at floor intersection joints, while the forces applied to the floor itself play a minor role. According to [13], the in-plane deformability of the first story has a greater effect than that of the upper ones. However, other studies show that this is not always true, due to the large increment in floor accelerations and the floor flexibility index along the building height ([9,11,19]). Hence, the shear distribution among vertical elements is investigated on all floors, testing the predictive capacity of the homogenization methods described in Sections 3.2, 3.3 and 3.4 with respect to the reference model with solid FE floors. The comparison with the results obtained by adopting rigid diaphragms is also provided.

The analyses' results are presented in terms of shear ratio v and its variation Δ_v at node A and C for each story. The shear ratio v is computed as $v = \frac{V^*}{V^{Story}}$, where V_{Story} is the resultant of the shear forces acting on the vertical elements of the story. The variation Δ_v is computed as $\Delta_v = \frac{v^* - v^{Ref}}{v^{Ref}}$.

The shear ratio in the wall, at each story and for each floor modeling approach, is shown in Table 5 and in Fig. 18 for the 1×4 floor cell structure, and in Table 7 and Fig. 20 for the 2×4 floor cell structure.

Looking at Fig. 18, it can be noticed that the shear ratio decreases with the story height passing from 0.232 to 0.173. Moreover, it is observed that the model with rigid diaphragm floors tends to overestimate the shear ratio, especially at the ground level (3.5 %) and the second-to-last story (4.0 %).

All the homogenization techniques accurately predict the shear ratio at the ground level, however, above for the upper stories the predictions are similar to those achieved with the rigid diaphragm model.

Looking then at Table 5, it is observed that, except for the last story, all the homogenization techniques well predict the shear forces in the wall ($\Delta_v \leq 3.1$ %).

Similarly, from Table 7 and Fig. 20 it is noticed that, for the 2×4 floor cell structure, all the homogenization techniques provide values of the shear ratio close to those of the reference model for all stories ($\Delta_v \leq$ 3.7 %), except for the last story. The shear ratio achieved by rigid diaphragms at ground level is slightly higher in 2×4 floor cell models (Δ_v

Table 3
Normalized displacements u and base shear forces v at nodes A and C, and in-plane relative drift Δ of the one-story 1 × 4 structure with floor joist along Y- and X-directions.

joists orientation	floor model	u_A	u_C	Δ	v_A	v_C	*err.* Δ	*err.* v_C
Y	Reference Model	1	1	5.81	1	1	0%	0%
	ANH	1.085	1.031	5.47	1.009	0.960	− 5.8%	− 4.0%
	SSH	1.086	1.029	5.45	1.010	0.958	− 6.2%	− 4.2%
	LFH	1.077	1.073	5.78	1.002	0.999	− 0.4%	+ 0.1%
	RC Slab	1.076	1.076	5.81	1.001	1.002	+ 0.1%	+ 0.2%
	Rigid diaphragm	1.244	0.183	0	1.164	0.169	–	− 83.1%
X	Reference Model	1	1	4.97	1	1	0%	0%
	ANH	0.991	0.985	4.93	1.007	0.954	− 0.8%	− 4.6%
	SSH	0.994	0.971	4.83	1.011	0.941	− 2.8%	− 5.9%
	LFH	0.980	1.059	5.45	0.996	1.027	+ 9.7%	+ 2.7%
	RC Slab	0.976	1.077	5.58	0.993	1.044	+ 12.3%	+ 4.4%
	Rigid diaphragm	1.123	0.188	0	1.148	0.182	–	− 81.8%

Table 4
Normalized displacements u and base shear forces v at nodes A and C, and in-plane relative drifts Δ of the one-story 2 × 4 structure with floor joist along Y- and X-directions.

joists orientation	floor model	u_A	u_C	Δ	v_A	v_C	$err.\Delta$	$err.\ v_C$
Y	Reference Model	1	1	2.58	1	1	0%	0%
	ANH	1.019	1.012	2.56	1.019	0.941	− 1.1%	− 5.9%
	SSH	1.019	1.015	2.57	1.018	0.943	− 0.5%	− 5.7%
	LFH	1.011	1.058	2.75	1.010	0.983	+ 6.5%	− 1.7%
	RC Slab	1.007	1.071	2.81	1.006	0.995	+ 8.9%	− 0.5%
	Rigid diaphragm	1.170	0.326	0	1.171	0.298	–	− 70.2%
X	Reference Model	1	1	2.41	1	1	0%	0%
	ANH	1.009	0.988	2.34	1.009	0.967	− 3.0%	− 3.3%
	SSH	1.010	0.986	2.33	1.009	0.964	− 3.3%	− 3.6%
	LFH	0.998	1.057	2.61	0.997	1.034	+ 8.3%	+ 3.4%
	RC Slab	0.993	1.084	2.73	0.992	1.061	+ 13.0%	+ 6.1%
	Rigid diaphragm	1.186	0.348	0	1.154	0.339	–	− 66.1%

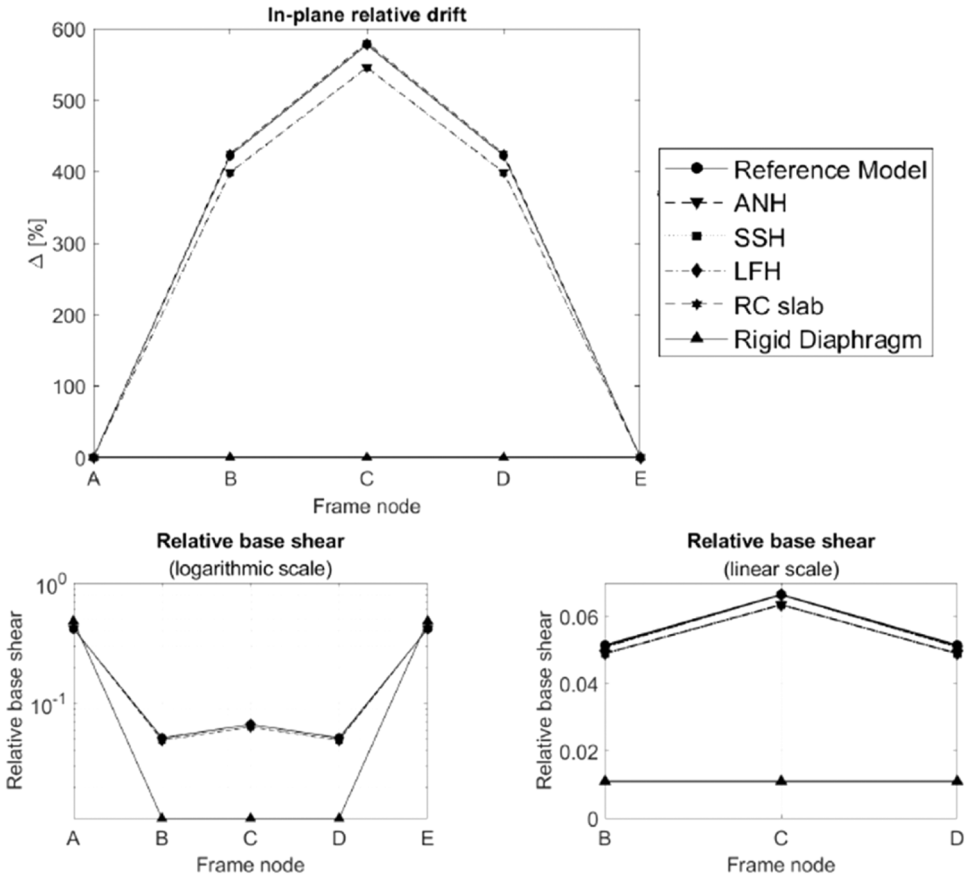

Fig. 17. In-plane relative drift Δ and relative base shear at nodes A, B, C, D, E of the one-story 1 × 4 structure with floor joists parallel to Y-direction.

=5.7 %) than in the 1×4 floor cell models (Δ_v = 3.5 %), and the inaccuracy of estimates increases for the two top stories where variations up to −14.3 % and to + 9.2 % are obtained.

Analogously, the shear ratio in the central column of the building, at each story and for each floor modeling approach, is shown in Table 6 and in Fig. 19 for the 1×4 floor cell structure, and in Table 8 and Fig. 21 for the 2×4 floor cell structure.

Looking at Fig. 19 and Fig. 21, it can be noticed that in both cases the shear ratio increases with the story height, passing from 0.013 to 0.055 and from 0.007 to 0.030 for 1×4 and 2×4 floor cell structures, respectively. It is also observed that the model with rigid diaphragm underestimates the shear ratio at every story the results obtained by and floors, it is possible to notice that rigid diaphragm models. The maximum error occurs at the ground level, where Δ_v is equal to −45.5 % and to −35.6 % for 1×4 and 2×4 floor cell structures, respectively.

Looking to the curves of the homogenized floor models, an acceptable estimate of the shear ratio is provided for the ground level, whereas, for the upper stories, the shear ratio tends to be similar to that achieved by the rigid diaphragm model.

Hence, noted that the floor in-plane displacement is more evident in the first floor for this kind of structure, the predictive capacity of the homogenization methods described in Sections 3.2, 3.3 and 3.4 is assessed more in detail for the first floor. To reduce the computational cost, in the reference model only the first story floor is modeled by solid elements, while the remaining floors are modeled using thin shell elements with the elastic properties obtained from the SSH homogenization approach.

The analyses' results are presented again in terms of normalized

Table 5
six-story building with 1 × 4 floor: shear ratio v and shear variation Δ_v at Node A at each floor.

CONSTANT LOADS											
joist orientation	Story	REFERENCE	ANH		SSH		LFH		RC Slab		Rigid Diaphragm	
		v	v	Δ_v	v	Δ_v	v	Δ_v	v	Δ_v	v	Δ_v
Y	1	0.232	0.233	0.5 %	0.233	0.5 %	0.233	0.4 %	0.233	0.4 %	0.240	3.5 %
	2	0.229	0.230	0.4 %	0.230	0.4 %	0.230	0.4 %	0.230	0.4 %	0.229	0.1 %
	3	0.220	0.224	1.6 %	0.224	1.7 %	0.224	1.7 %	0.224	1.7 %	0.224	1.4 %
	4	0.213	0.218	2.2 %	0.218	2.3 %	0.218	2.3 %	0.218	2.3 %	0.218	2.2 %
	5	0.203	0.209	3.0 %	0.210	3.1 %	0.210	3.1 %	0.210	3.1 %	0.210	3.5 %
	6	0.170	0.183	7.3 %	0.183	7.3 %	0.183	7.5 %	0.183	7.6 %	0.174	2.2 %
X	1	0.232	0.234	0.7 %	0.234	0.8 %	0.233	0.5 %	0.233	0.4 %	0.240	3.4 %
	2	0.228	0.230	1.1 %	0.230	1.1 %	0.230	1.0 %	0.230	1.0 %	0.229	0.7 %
	3	0.221	0.224	1.4 %	0.224	1.4 %	0.224	1.5 %	0.224	1.5 %	0.224	1.2 %
	4	0.214	0.218	1.8 %	0.218	1.8 %	0.218	1.9 %	0.218	1.9 %	0.218	1.8 %
	5	0.204	0.209	2.6 %	0.209	2.6 %	0.210	2.6 %	0.209	2.6 %	0.210	3.0 %
	6	0.173	0.182	5.2 %	0.182	5.2 %	0.183	5.6 %	0.183	5.7 %	0.174	0.4 %
LINEAR LOADS												
joist orientation	Story	REFERENCE	ANH		SSH		LFH		RC Slab		Rigid Diaphragm	
		v	v	Δ_v	v	Δ_v	v	Δ_v	v	Δ_v	v	Δ_v
Y	1	0.235	0.236	0.5 %	0.236	0.5 %	0.236	0.4 %	0.236	0.4 %	0.239	1.9 %
	2	0.227	0.228	0.4 %	0.228	0.5 %	0.228	0.4 %	0.228	0.4 %	0.228	0.7 %
	3	0.219	0.222	1.4 %	0.223	1.5 %	0.222	1.4 %	0.222	1.4 %	0.224	1.9 %
	4	0.214	0.218	1.9 %	0.218	1.9 %	0.218	1.9 %	0.218	1.9 %	0.219	2.7 %
	5	0.206	0.211	2.5 %	0.211	2.6 %	0.211	2.5 %	0.211	2.5 %	0.214	4.0 %
	6	0.179	0.189	5.7 %	0.189	5.8 %	0.189	5.8 %	0.189	5.9 %	0.186	3.9 %
X	1	0.235	0.236	0.7 %	0.237	0.7 %	0.236	0.6 %	0.236	0.6 %	0.239	2.0 %
	2	0.226	0.228	1.0 %	0.228	1.0 %	0.228	1.0 %	0.228	1.0 %	0.228	1.2 %
	3	0.220	0.222	1.3 %	0.223	1.3 %	0.223	1.3 %	0.222	1.3 %	0.224	1.8 %
	4	0.214	0.218	1.6 %	0.218	1.7 %	0.218	1.6 %	0.218	1.6 %	0.219	2.3 %
	5	0.206	0.211	2.1 %	0.211	2.3 %	0.211	2.2 %	0.211	2.1 %	0.214	3.6 %
	6	0.181	0.189	4.1 %	0.189	4.2 %	0.189	4.2 %	0.189	4.3 %	0.186	2.2 %

Table 6
six-story building with 1 × 4 floor: shear ratio v and shear variation Δ_v at Node C at each floor.

CONSTANT LOADS											
joist orientation	Story	REFERENCE	ANH		SSH		LFH		RC Slab		Rigid Diaphragm	
		v	v	Δ_v	v	Δ_v	v	Δ_v	v	Δ_v	v	Δ_v
Y	1	0.013	0.012	−6.7 %	0.012	−6.9 %	0.012	−4.8 %	0.012	−4.5 %	0.007	−49.5 %
	2	0.015	0.014	−6.8 %	0.013	−7.2 %	0.014	−6.7 %	0.014	−6.9 %	0.014	−3.3 %
	3	0.020	0.018	−13.5 %	0.018	−13.8 %	0.018	−13.9 %	0.018	−13.9 %	0.018	−11.5 %
	4	0.026	0.022	−14.8 %	0.022	−15.1 %	0.022	−15.2 %	0.022	−15.2 %	0.022	−14.3 %
	5	0.033	0.028	−15.8 %	0.028	−16.0 %	0.028	−16.1 %	0.028	−16.0 %	0.027	−17.6 %
	6	0.055	0.046	−16.7 %	0.046	−16.8 %	0.046	−17.4 %	0.045	−17.6 %	0.053	−3.6 %
X	1	0.011	0.010	−7.8 %	0.010	−8.1 %	0.010	−6.8 %	0.010	−6.6 %	0.007	−33.0 %
	2	0.016	0.015	−6.0 %	0.015	−6.4 %	0.015	−5.9 %	0.015	−6.0 %	0.015	−8.7 %
	3	0.021	0.019	−11.3 %	0.019	−11.6 %	0.019	−11.3 %	0.019	−11.3 %	0.018	−15.7 %
	4	0.026	0.022	−12.9 %	0.022	−13.1 %	0.022	−12.8 %	0.022	−12.8 %	0.021	−18.1 %
	5	0.032	0.027	−14.0 %	0.027	−14.2 %	0.027	−13.9 %	0.028	−13.8 %	0.025	−21.9 %
	6	0.050	0.042	−15.0 %	0.042	−15.3 %	0.042	−15.4 %	0.042	−15.6 %	0.045	−9.6 %
LINEAR LOADS												
joist orientation	Story	REFERENCE	ANH		SSH		LFH		RC Slab		Rigid Diaphragm	
		v	v	Δ_v	v	Δ_v	v	Δ_v	v	Δ_v	v	Δ_v
Y	1	0.013	0.012	−9.1 %	0.012	−9.7 %	0.012	−5.5 %	0.012	−4.5 %	0.007	−49.0 %
	2	0.015	0.013	−11.5 %	0.013	−11.7 %	0.014	−10.9 %	0.014	−10.9 %	0.014	−7.5 %
	3	0.020	0.018	−11.3 %	0.018	−11.2 %	0.018	−11.6 %	0.018	−11.5 %	0.018	−9.2 %
	4	0.025	0.022	−11.5 %	0.022	−11.5 %	0.022	−11.7 %	0.022	−11.7 %	0.022	−10.9 %
	5	0.032	0.028	−12.3 %	0.028	−12.2 %	0.028	−12.5 %	0.028	−12.4 %	0.027	−14.2 %
	6	0.053	0.046	−12.5 %	0.046	−12.4 %	0.046	−13.5 %	0.045	−13.8 %	0.053	0.7 %
X	1	0.011	0.010	−11.1 %	0.010	−11.4 %	0.010	−8.9 %	0.010	−8.3 %	0.007	−34.0 %
	2	0.017	0.015	−9.9 %	0.015	−10.1 %	0.015	−9.4 %	0.015	−9.3 %	0.015	−11.7 %
	3	0.021	0.019	−9.3 %	0.019	−10.0 %	0.019	−9.6 %	0.019	−9.4 %	0.018	−13.9 %
	4	0.025	0.022	−9.7 %	0.022	−10.5 %	0.022	−9.9 %	0.022	−9.7 %	0.021	−15.1 %
	5	0.031	0.027	−10.5 %	0.027	−11.2 %	0.027	−10.6 %	0.027	−10.4 %	0.025	−18.7 %
	6	0.048	0.042	−11.3 %	0.042	−11.6 %	0.042	−11.8 %	0.042	−12.0 %	0.045	−5.6 %

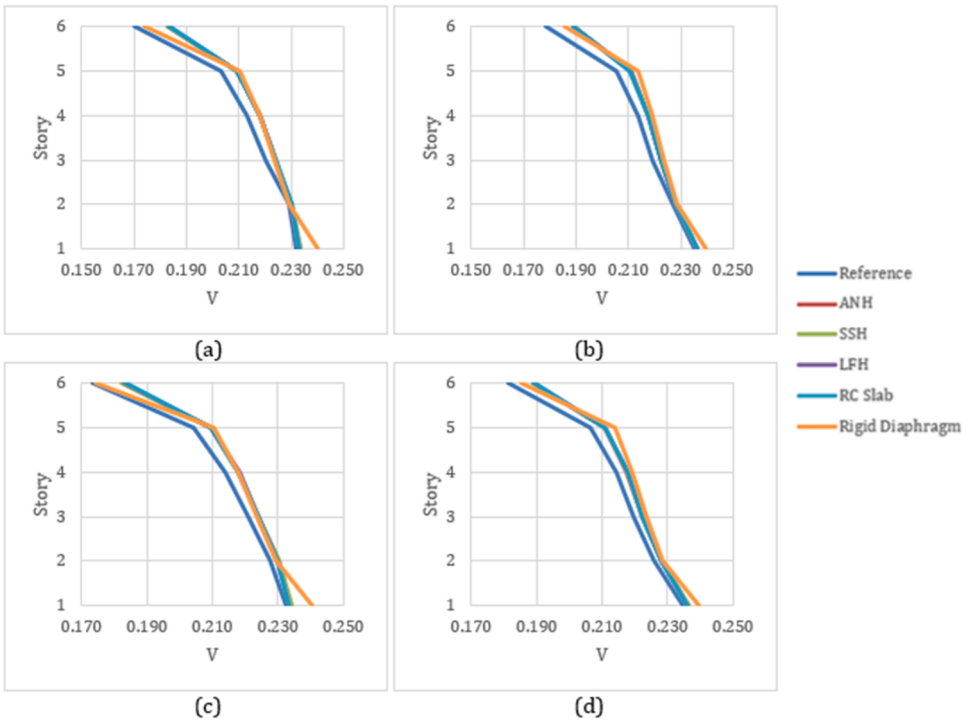

Fig. 18. six-story building with 1 × 4 floor: shear ratio v at node A at each story, for Y joist orientation with constant load (a) and linear load pattern (b), for X joist orientation with constant load (c) and linear load pattern (d).

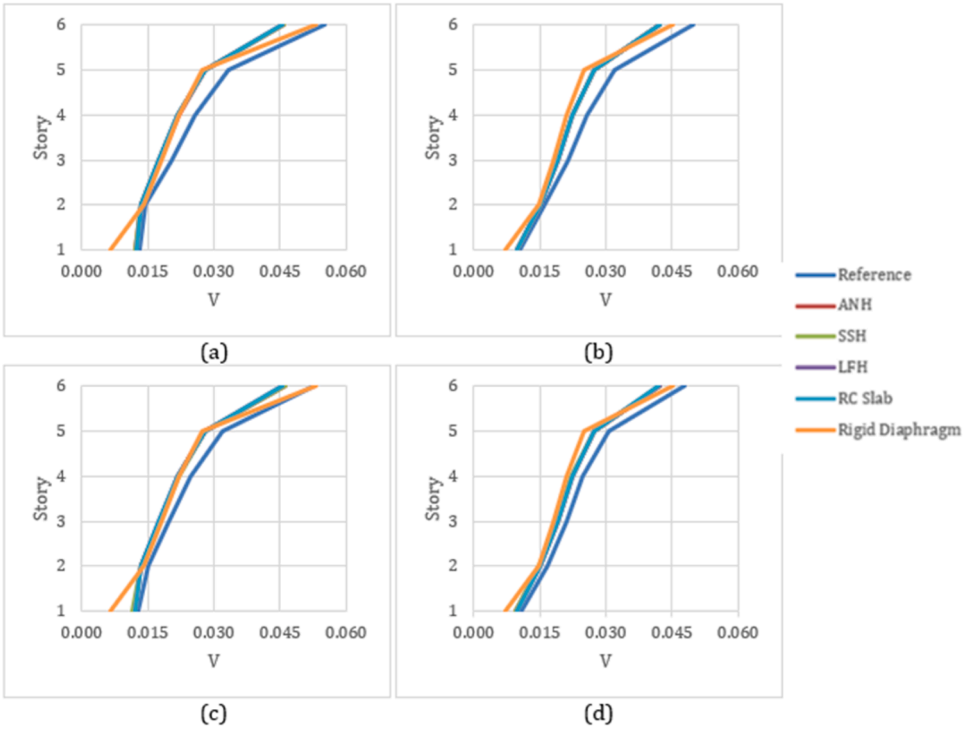

Fig. 19. six-story building with 1 × 4 floor: shear ratio v at node C at each story, for Y joist orientation with constant load (a) and linear load pattern (b), for X joist orientation with constant load (c) and linear load pattern (d).

displacements u, normalized shears v at the base of columns, and walls and normalized story drifts Δ at nodes A and C of the first floor, and they are reported in Table 9 and Table 10.

From these tables it can be seen that there is a remarkable decrease in the relative drifts Δ of the first story of the six-story structure, compared to those of the one-story structures (Tables 3 and 4). For instance, the normalized drift value Δ of the reference building with 1 × 4 floor for the constant load distribution passes from 581% for the one-story structure (Table 3) to 67% for the six-story structure (Table 9), an 88 % reduction in Δ. The decrease is even greater (a 94%. reduction) for the linear load distribution. For the 2 × 4 floor configuration, the decreases in the first story drifts are very similar to those of the corresponding strucure with

Table 7
six-story building with 2 × 4 floor: shear ratio v and shear variation Δ_v at Node A at each floor.

CONSTANT LOADS											
joist orientation	Story	REFERENCE	ANH		SSH		LFH		RC Slab		Rigid Diaphragm	
		V	V	Δ_V	V	Δ_V	V	Δ_V	V	Δ_V	V	Δ_V
Y	1	0.140	0.142	1.1 %	0.142	1.1 %	0.141	0.8 %	0.141	0.8 %	0.148	5.7 %
	2	0.127	0.128	1.0 %	0.128	1.0 %	0.128	1.0 %	0.128	1.1 %	0.126	−1.0 %
	3	0.115	0.116	1.1 %	0.116	1.1 %	0.116	1.1 %	0.116	1.2 %	0.116	0.9 %
	4	0.106	0.108	1.8 %	0.108	1.8 %	0.108	1.8 %	0.108	1.8 %	0.106	0.7 %
	5	0.092	0.096	3.7 %	0.096	3.7 %	0.096	3.5 %	0.096	3.5 %	0.101	9.2 %
	6	0.039	0.045	14.0 %	0.044	13.8 %	0.045	15.4 %	0.045	15.7 %	0.034	−13.9 %
X	1	0.140	0.142	1.3 %	0.142	1.4 %	0.142	1.1 %	0.141	1.0 %	0.148	5.9 %
	2	0.127	0.128	0.5 %	0.128	0.5 %	0.128	0.5 %	0.128	0.5 %	0.126	−1.5 %
	3	0.115	0.116	0.9 %	0.116	0.9 %	0.116	0.9 %	0.116	1.0 %	0.115	0.4 %
	4	0.106	0.108	1.5 %	0.108	1.5 %	0.108	1.5 %	0.108	1.5 %	0.107	1.2 %
	5	0.093	0.096	3.1 %	0.096	3.1 %	0.096	3.0 %	0.096	3.0 %	0.100	7.3 %
	6	0.040	0.045	10.6 %	0.045	10.6 %	0.045	11.9 %	0.045	12.2 %	0.035	−14.3 %
LINEAR LOADS												
joist orientation	Story	REFERENCE	ANH		SSH		LFH		RC Slab		Rigid Diaphragm	
		V	V	Δ_V	V	Δ_V	V	Δ_V	V	Δ_V	V	Δ_V
Y	1	0.141	0.142	1.1 %	0.142	1.1 %	0.142	0.9 %	0.142	0.9 %	0.147	4.1 %
	2	0.125	0.126	0.8 %	0.126	0.8 %	0.126	0.9 %	0.126	0.9 %	0.124	−0.3 %
	3	0.115	0.116	0.9 %	0.116	0.9 %	0.116	0.9 %	0.116	0.9 %	0.116	1.3 %
	4	0.108	0.110	1.5 %	0.110	1.5 %	0.110	1.5 %	0.110	1.4 %	0.109	1.2 %
	5	0.098	0.101	3.0 %	0.101	3.0 %	0.101	2.7 %	0.100	2.7 %	0.106	8.5 %
	6	0.054	0.058	8.6 %	0.058	8.5 %	0.059	9.3 %	0.059	9.4 %	0.051	−5.9 %
X	1	0.142	0.142	0.7 %	0.142	0.7 %	0.142	0.5 %	0.142	0.5 %	0.147	3.6 %
	2	0.125	0.126	0.5 %	0.126	0.5 %	0.126	0.5 %	0.126	0.5 %	0.124	−0.7 %
	3	0.115	0.116	0.8 %	0.116	0.8 %	0.116	0.8 %	0.116	0.8 %	0.116	1.0 %
	4	0.108	0.110	1.3 %	0.110	1.3 %	0.110	1.3 %	0.110	1.2 %	0.110	1.6 %
	5	0.098	0.101	2.5 %	0.101	2.5 %	0.101	2.3 %	0.101	2.3 %	0.105	7.1 %
	6	0.055	0.059	6.2 %	0.058	6.2 %	0.059	6.8 %	0.059	6.8 %	0.051	−7.1 %

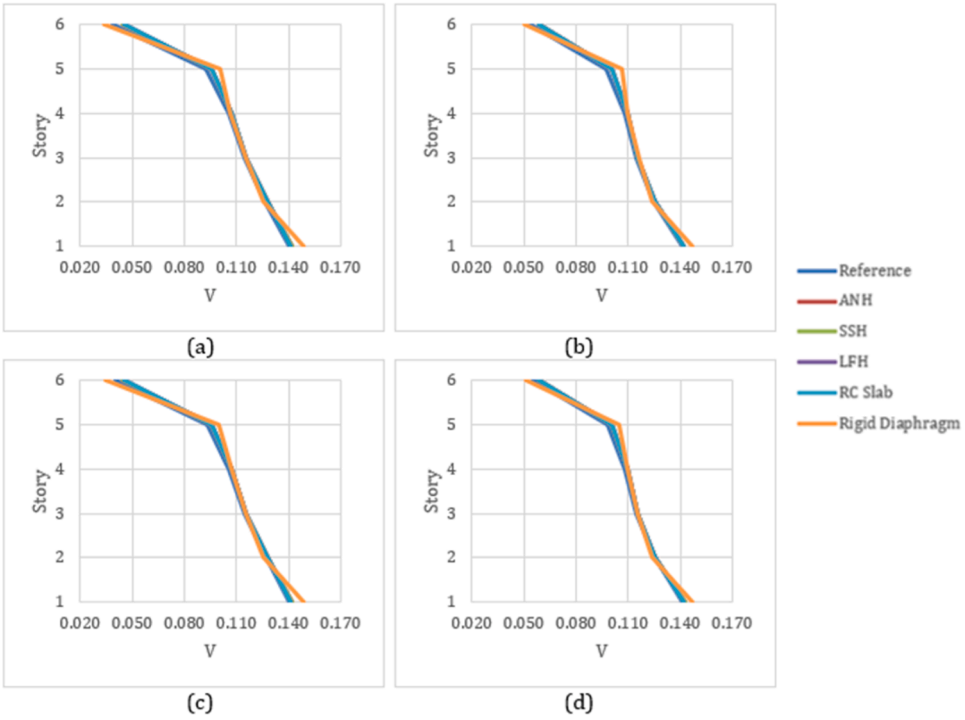

Fig. 20. six-story building with 2 × 4 floor: shear ratio v at node A at each story, for Y joist orientation with constant load (a) and linear load pattern (b), for X joist orientation with constant load (c) and linear load pattern (d).

Table 8
six-story building with 2 × 4 floor: shear ratio v and shear variation Δ_v at Node C at each floor.

CONSTANT LOADS											
joist orientation	Story	REFERENCE	ANH		SSH		LFH		RC Slab		Rigid Diaphragm	
		V	V	Δ_V	V	Δ_V	V	Δ_V	V	Δ_V	V	Δ_V
Y	1	0.007	0.007	−8.4 %	0.007	−8.3 %	0.007	−6.7 %	0.007	−6.1 %	0.005	−35.6 %
	2	0.011	0.010	−10.3 %	0.010	−10.3 %	0.010	−10.1 %	0.010	−10.2 %	0.010	−7.5 %
	3	0.014	0.012	−10.7 %	0.012	−10.8 %	0.012	−10.9 %	0.012	−11.0 %	0.013	−8.1 %
	4	0.016	0.014	−10.9 %	0.014	−10.9 %	0.014	−11.0 %	0.014	−11.0 %	0.015	−10.4 %
	5	0.020	0.017	−12.5 %	0.017	−12.5 %	0.017	−12.5 %	0.017	−12.5 %	0.017	−14.6 %
	6	0.030	0.026	−13.7 %	0.026	−13.8 %	0.026	−14.3 %	0.026	−14.6 %	0.029	−3.2 %
X	1	0.007	0.007	−5.6 %	0.007	−5.7 %	0.007	−3.0 %	0.007	−1.9 %	0.005	−32.4 %
	2	0.011	0.010	−7.2 %	0.010	−7.3 %	0.010	−7.0 %	0.010	−6.9 %	0.010	−4.1 %
	3	0.013	0.012	−7.9 %	0.012	−7.9 %	0.012	−8.2 %	0.012	−8.3 %	0.013	−5.4 %
	4	0.016	0.014	−8.6 %	0.014	−8.6 %	0.014	−8.7 %	0.014	−8.8 %	0.015	−8.2 %
	5	0.019	0.017	−9.6 %	0.017	−9.6 %	0.017	−9.6 %	0.017	−9.6 %	0.017	−11.8 %
	6	0.029	0.026	−10.4 %	0.026	−10.4 %	0.026	−11.2 %	0.026	−11.6 %	0.029	0.2 %
LINEAR LOADS											
joist orientation	Story	REFERENCE	ANH		SSH		LFH		RC Slab		Rigid Diaphragm	
		V	V	Δ_V	V	Δ_V	V	Δ_V	V	Δ_V	V	Δ_V
Y	1	0.007	0.006	−9.0 %	0.006	−8.9 %	0.006	−7.9 %	0.006	−7.5 %	0.005	−25.0 %
	2	0.012	0.010	−8.8 %	0.010	−8.8 %	0.011	−8.6 %	0.011	−8.6 %	0.011	−8.6 %
	3	0.014	0.013	−9.4 %	0.013	−9.4 %	0.013	−9.3 %	0.013	−9.3 %	0.012	−10.5 %
	4	0.016	0.014	−10.0 %	0.014	−9.9 %	0.014	−9.7 %	0.014	−9.7 %	0.014	−12.4 %
	5	0.019	0.016	−11.6 %	0.016	−11.5 %	0.016	−11.3 %	0.017	−11.2 %	0.015	−17.0 %
	6	0.027	0.024	−13.1 %	0.024	−13.1 %	0.024	−13.3 %	0.024	−13.5 %	0.025	−7.1 %
X	1	0.007	0.006	−6.9 %	0.006	−7.0 %	0.006	−5.4 %	0.006	−4.7 %	0.005	−22.6 %
	2	0.011	0.010	−6.8 %	0.010	−6.8 %	0.010	−6.5 %	0.010	−6.4 %	0.011	−6.3 %
	3	0.014	0.013	−7.5 %	0.013	−7.6 %	0.013	−7.4 %	0.013	−7.4 %	0.012	−8.5 %
	4	0.016	0.014	−8.1 %	0.014	−8.1 %	0.014	−7.8 %	0.014	−7.7 %	0.014	−10.4 %
	5	0.018	0.016	−9.3 %	0.016	−9.3 %	0.016	−8.9 %	0.016	−8.7 %	0.015	−14.5 %
	6	0.026	0.024	−9.9 %	0.024	−10.0 %	0.024	−10.2 %	0.024	−10.4 %	0.025	−3.7 %

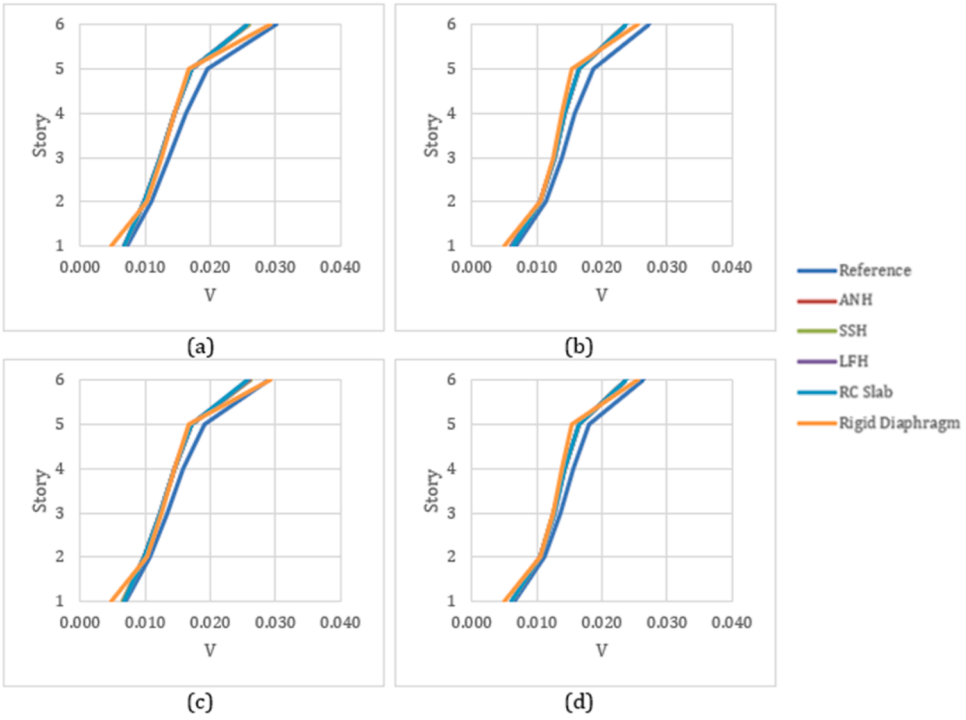

Fig. 21. six-story building with 2 × 4 floor: shear ratio v at node C at each story, for Y joist orientation with constant load (a) and linear load pattern (b), for X joist orientation with constant load (c) and linear load pattern (d).

Table 9
six-story building with 1 × 4 floor: normalized displacements u, and base shear forces v at nodes A and C, and in-plane relative drifts Δ.

CONSTANT LOADS								
joist orientation	floor model	u_A	u_C	Δ	v_A	v_C	err. Δ	err. v_C
Y	REFERENCE	1	1	0.67	1	1	0.0 %	0.0 %
	ANH	1.059	1.000	0.60	1.005	0.933	−9.9 %	−6.7 %
	SSH	1.060	0.999	0.60	1.005	0.931	−9.9 %	−6.9 %
	LFH	1.059	1.016	0.63	1.004	0.952	−5.4 %	−4.8 %
	RC Slab	1.060	1.020	0.64	1.004	0.955	−4.0 %	−4.5 %
	Rigid Diaphragm	1.075	0.627	0	1.035	0.505	–	−49.5 %
X	REFERENCE	1	1	0.59	1	1	0.0 %	0.0 %
	ANH	0.983	0.946	0.55	1.007	0.909	−5.6 %	−9.1 %
	SSH	0.983	0.941	0.55	1.008	0.903	−6.8 %	−9.7 %
	LFH	0.982	0.973	0.60	1.005	0.945	1.3 %	−5.5 %
	RC Slab	0.982	0.987	0.62	1.004	0.955	6.3 %	−4.5 %
	Rigid Diaphragm	0.995	0.612	0	1.034	0.510	–	−49.0 %
LINEAR LOADS								
joist orientation	floor model	u_A	u_C	Δ	v_A	v_C	err. Δ	err. v_C
Y	REFERENCE	1	1	0.32	1	1	0.0 %	0.0 %
	ANH	1.060	0.993	0.27	1.005	0.922	−17.2 %	−7.8 %
	SSH	1.061	0.993	0.27	1.005	0.919	−17.2 %	−8.1 %
	LFH	1.061	1.002	0.28	1.004	0.932	−14.0 %	−6.8 %
	RC Slab	1.061	1.005	0.29	1.004	0.934	−11.0 %	−6.6 %
	Rigid Diaphragm	1.069	0.785	0	1.019	0.670	–	−33.0 %
X	REFERENCE	1	1	0.28	1	1	0.0 %	0.0 %
	ANH	0.984	0.934	0.25	1.007	0.889	−12.6 %	−11.1 %
	SSH	0.985	0.932	0.25	1.007	0.886	−13.5 %	−11.4 %
	LFH	0.984	0.949	0.27	1.006	0.911	−6.2 %	−8.9 %
	RC Slab	0.983	0.958	0.28	1.006	0.917	−0.7 %	−8.3 %
	Rigid Diaphragm	0.991	0.750	0	1.020	0.660	–	−34.0 %

Table 10
six-story building with 2 × 4 floor: normalized displacements u and base shear forces v at nodes A and C, and in-plane relative drifts Δ.

CONSTANT LOADS								
joist orientation	floor model	u_A	u_C	Δ	v_A	v_C	err. Δ	err. v_C
Y	REFERENCE	1	1	0.34	1	1	0.0 %	0.0 %
	ANH	0.994	0.974	0.33	1.011	0.916	−3.2 %	−8.4 %
	SSH	0.994	0.975	0.33	1.011	0.917	−2.7 %	−8.3 %
	LFH	0.994	0.987	0.35	1.008	0.933	2.0 %	−6.7 %
	RC Slab	0.993	0.994	0.36	1.008	0.939	5.5 %	−6.1 %
	Rigid Diaphragm	0.999	0.704	0	1.057	0.644	–	−35.6 %
X	REFERENCE	1	1	0.32	1	1	0.0 %	0.0 %
	ANH	0.998	0.971	0.31	1.013	0.944	−4.4 %	−5.6 %
	SSH	0.998	0.970	0.31	1.014	0.943	−4.4 %	−5.7 %
	LFH	0.997	0.990	0.33	1.011	0.970	3.1 %	−3.0 %
	RC Slab	0.996	1.002	0.36	1.010	0.981	9.5 %	−1.9 %
	Rigid Diaphragm	1.015	0.753	0	1.059	0.676	–	−32.4 %
LINEAR LOADS								
joist orientation	floor model	u_A	u_C	Δ	v_A	v_C	err. Δ	err. v_C
Y	REFERENCE	1	1	0.18	1	1	0.0 %	0.0 %
	ANH	0.994	0.968	0.17	1.011	0.910	−7.5 %	−9.0 %
	SSH	0.994	0.968	0.17	1.011	0.911	−7.0 %	−8.9 %
	LFH	0.994	0.975	0.18	1.009	0.921	−2.7 %	−7.9 %
	RC Slab	0.993	0.979	0.18	1.009	0.925	1.1 %	−7.5 %
	Rigid Diaphragm	0.982	0.791	0	1.041	0.750	–	−25.0 %
X	REFERENCE	1	1	0.17	1	1	0.0 %	0.0 %
	ANH	0.992	0.958	0.16	1.007	0.931	−9.1 %	−6.9 %
	SSH	0.992	0.957	0.16	1.007	0.930	−9.0 %	−7.0 %
	LFH	0.991	0.969	0.17	1.005	0.946	−2.1 %	−5.4 %
	RC Slab	0.991	0.975	0.18	1.005	0.953	4.3 %	−4.7 %
	Rigid Diaphragm	1.003	0.849	0	1.036	0.774	–	−22.6 %

1 × 4 floor configuration.

It is also worth noting that, despite having a low level of in-plane flexibility, the rigid floor model still heavily underestimates the reference floor displacement and shear at the base of the mid-side column. For instance, the base shear at node C is between 50% and 80% of the reference model shear.

Regarding the performance of the considered homogenization methods, they are all deemed suitable to predict the reference floor behavior, since the errors in terms of both displacements (u) and base shears (v) are always well below 12%.

Regarding the RC Slab model, in which the floor is modeled by the reinforced concrete slab only, it resulted that, for both of the two six-story structures and for each of the load patterns, the maximum error is around 8.5 % both for displacements and base shears, making this model the first choice for its efficiency and simplicity.

5. Conclusions

In this study, the issue of reproducing, in the FE models of buildings, the in-plane flexibility of complex floor systems through equivalent orthotropic slabs has been addressed. In particular, to derive the elastic parameters of the equivalent slab representing the in-plane behavior of a single floor cell, three different homogenization methods have been used. Two of these methods, SSH and LFH, are based on the comparison between the two FE models of the floor cell made with solid and shell elements, respectively. By contrast, in the third method, ANH, the elastic properties are analytically derived. The capacity of the three methods in predicting both floor deformability and base shears in vertical structural members has been assessed on two one-story and two six-story buildings, with lateral shear walls and with floor aspect ratios equal to 4:1 and 2:1. From the performed analyses, the following conclusions are drawn.

1. The most important parameter driving the in-plane flexibility of the equivalent orthotropic slab is the in-plane shear modulus G, while the extensional moduli, E_1 and E_2, play a minor role. Notably, varying the value of E_1 in the range 20 to 70 GPa, the floor displacements and base shears vary by only 4.16% and 8.36% for the cases with joists parallel to the X-direction (E_1 dominant) or the Y-direction (E_2 dominant), respectively.
2. For the considered case studies, the three homogenization methods produce results that are very close each other.
3. Moreover, all the methods are suitable to reproduce the reference floor in-plane behavior, since the errors both on displacements and base shear predictions are always well below 10% with respect to the reference model.
4. On the basis of the above, among the considered homogenization methods, it is suggested that the first choice be the analytical method (ANH), which is the simplest one and does not require modeling the floor with solid FEs, thereby avoiding computational effort.
5. The rigid diaphragm assumption is inadequate to represent floors' in-plane behavior in the considered buildings, since it underestimates the base shear in internal columns. In particular, for the one-story structures, the base shear is less than one-fifth the reference shear for the building with 4:1 floor aspect ratio, and about one-third the reference shear for the case with 2:1 aspect ratio.
6. In the cases in which floors' in-plane flexibility is modeled taking account of only the top RC slab, good results are obtained both in terms of relative drifts (Δ) and base shears (v). With this model, the largest error on Δ is around 11 %, while the largest error on v is 8.3 %. It is concluded that the use of a homogenization procedure is not strictly necessary to accurately reproduce the in-plane behavior of RC floors with joists and a slab on the top. This outcome is of great relevance for the study of Italian existing RC buildings, for which the composition of the floors is not always known.

Declaration of Competing Interest

The authors declare the following financial interests/personal relationships which may be considered as potential competing interests Margherita Pauletta reports financial support was provided by Italian Department of Civil Protection and by the University of Udine. Giada Frappa reports financial support was provided by European Union NextGenerationEU.

Acknowledgements

The research has been partially funded by:

1. the Italian Department of Civil Protection, within the framework of Executive Project DPCReLUIS 2022–2024,

2. iNEST Interconnected Northeast Innovation Ecosystem research program, from the resources of the National Plan for Recovery and Resilience (NRP), M4C2 -investment 1.5. Creation and strengthening of "Innovation Ecosystems for Sustainability", funded by the European Union, NextGenerationEU, CUP F43C22000200006.

3. the strategic plan of University of Udine within the framework of the project "ESPeRT", whose support is greatly appreciated.

References

[1] Cohen GL, Klingner RE, Hayes JR, Seeney SC. Seismic evaluation of low-rise reinforced masonry buildings with flexible diaphragms: III. Synthesis and application. Earthq Spectra 2006;22:329–47.
[2] Koliou M, Filiatrault A, Kelly DJ, Lawson J. Buildings with rigid walls and flexible roof diaphragms. I: evaluation of current U.S. seismic provisions. J Struct Eng 2016;142(3):04015166.
[3] Betti M, Galano L, Vignoli A. Comparative analysis on the seismic behavior of unreinforced masonry buildings with flexible diaphragms. Eng Struct 2014;61:195–208.
[4] Kollerathu JA, Menon A. Role of diaphragm flexibility modelling in seismic analysis of existing masonry structures. Structures 2017;11:22–39.
[5] Whitney R, Agrawal AK. Seismic performance of flexible timber diaphragms: damping, force–displacement and natural period. Eng Struct 2015;101:583–90.
[6] Diaferio M, Foti D, Giannoccaro NI, Ivorra S. Optimal model through identified frequencies of a masonry building structure with wooden floors. Int J Mech 2014;8(1):282–8.
[7] Diaferio M, Foti D, Giannoccaro NI, Sabbà MF. Dynamic identification on an irregular structure. Appl Sci 2022;12:3445.
[8] Celebi M, Buongiovanni G, Safak E, Brady G. Seismic response of a large-span roof diaphragm. Earthq Spectra 1989;5:337–50.
[9] Tena-Colunga A. Seismic evaluation of unreinforced masonry structures with flexible diaphragms. Earthq Spectra 1992;8:305–18.
[10] Tena-Colunga A, Abrams DP. Simplified 3-D dynamic analysis of structures with flexible diaphragms. Earthq Eng Struct Dyn 1995;24:221–32.
[11] Tena-Colunga A, Abrams DP. Response of an Unreinforced Masonry Building During the Loma Prieta Earthquake. Earthquake Engineering, Tenth world Conference. Rotterdam: Balkema; 1992. p. 79–84.
[12] Tena-Colunga A, Abrams DP. Seismic behavior of structures with flexible diaphragms. J Struct Eng 1996:439–45.
[13] Saffarini HS, Qudaimat MM. In-plane floor deformations in RC structures. J Struct Eng 1992;118(11):3089–102.
[14] Ruggieri S, Porco F, Uva G. A practical approach for estimating the floor deformability in existing RC buildings: evaluation of the effects in the structural response and seismic fragility. Bull Earthq Eng 2020;18:2083–113.
[15] Tena-Colunga A, Chinchilla-Portillo KL, Juárez-Luna G. Assessment of the diaphragm condition for floor systems used in urban buildings. Eng Struct 2015;93:70–84.
[16] Ju SH, Lin MC. Comparison of building analyses assuming rigid or flexible floors. J Struct Eng 1999;125(1):25–31.
[17] Basu D, Jain SK. Seismic analysis of asymmetric buildings with flexible floor diaphragms. J Struct Eng 2004;130(8):1169–76.
[18] Fang C, Leon RT. Seismic behavior of symmetric and asymmetric steel structures with rigid and semirigid diaphragms. J Struct Eng 2018;144(10):04018186.
[19] Tena-Colunga A, Sabanero-Garcia R. Impact of diaphragm flexibility on dynamic properties and seismic design parameters of irregular buildings in plan. J Build Eng 2023;80:108007.
[20] Eivani H., Moghadam A.S., Aziminejad A., Nekooei M. Seismic Response of Plan-Asymmetric Structures with Diaphragm Flexibility. Shock and Vibration 2018; ID4149212.
[21] Sadashiva VK, MacRae GA, Deam BL, Spooner MS. Quantifying the seismic response of structures with flexible diaphragms. Earthq Eng Struct Dyn 2012;41:1365–89.
[22] Eivani H, Tena-Colunga A, Moghadam AS. Proper configuration of stiffness and strength centers in asymmetric single-story structures with semi-flexible diaphragms. Structures 2022;40:149–62.
[23] Masi A, Dolce M, Caterina F. Seismic response of irregular multi-storey buildings with flexible inelastic diaphragms. Struct Des Tall Build 1997;6:99–124.
[24] Khajehdehi R, Panahshahi N. Effect of openings on in-plane structural behavior of reinforced concrete floor slabs. J Build Eng 2016;7:1–11.
[25] Kalib E.S., Shewalul Y.W. Response of the Flat Reinforced Concrete Floor Slab with Openings under Cyclic In-Plane Loading. Advances in Civil Engineering 2021; ID 2503475.
[26] Fleischman RB, Farrow KT. Dynamic behavior of perimeter lateral-system structures with flexible diaphragms. Earthq Eng Struct Dyn 2001;30:745–63.
[27] Kunnath SK, Panahshahi N, Reinhorn AM. Seismic response of RC buildings with inelastic floor diaphragms. J Struct Eng 1991;117(4):1218–37.

[28] European Committee for Standardization (CEN), UNI EN 1998–1:2005. Eurocode 8 - Earthquake resistant design of structures - Part I: General rules, seismic action and rules for buildings. Brussels, Belgium, 2005.
[29] Standards New Zealand, New Zealand Standard (NZS) 1170.5 Supp 1:2004. Structural Design Actions. Part 5: Earthquake actions New Zealand - Commentary. 2004.
[30] Earthquake Planning and Protection Organization, Greek Seismic Code. Earthquake resistant design of structures. Earthquake Planning and Protection. Athens, 2000.
[31] Seismology Committee Structural Engineers Association of California, Structural Engineers Association of California (SEAOC). Recommended Lateral Force Requirements and Commentary. Seventh Edition; Sacramento, California, 1999.
[32] Building Seismic Safety Council, National Institute of building sciences, FEMA 450. National earthquake hazards reduction program recommended provision for seismic regulations for new buildings and other structures. Washington, 2003.
[33] American Society of Civil Engineers, ASCE/SEI 7–10. Minimum Design Loads for Building and Other Structures. 2nd edn.; 1801 Alexander Bell Drive, Reston, 2002: 20191–24400.
[34] Ministry of Housing and Urban Development, Standard no2700–05. Iranian Code of Practice for Seismic Resistant Design of Building. 3rd Edition; 2007.
[35] Troitsky MS. Stiffened plates: bending, stability and vibrations. Amsterdam; New York: Elsevier Scientific Pub. Co,; 1976.
[36] Staszak N, Garbowski T, Szymczak-Graczyk A. Solid truss to shell numerical homogenization of prefabricated composite slabs. Materials 2021;14:4120.
[37] Staszak N, Garbowski T, Ksit B. Optimal design of bubble deck concrete slabs: sensitivity analysis and numerical homogenization. Materials 2023;16.
[38] Biancolini ME. Evaluation of equivalent stiffness properties of corrugated board. Comp Struct 2005;69:322–8.
[39] Pecce M, Ceroni F, Maddaloni G, Iannuzzella V. Assessment of the in-plane deformability of RC floors with traditional and innovative lightening elements in RC framed and wall structures. Bull Earthq Eng 2017;15:3125–49.
[40] Ruggieri S, Porco F, Uva G. A numerical procedure of modeling the floor deformability in seismic analysis of existing RC buildings. J Build Eng 2018;19: 273–84.
[41] Foti D, Giannocaro NI, Sabbà MF, La Scala A. Dynamic identification of a strategic building of the sixties with a mixed structure. Procedia Struct Integr 2023;44: 782–9.
[42] Clyne TW, Hull D. An introduction to composite materials, third edition. Cambridge University Press,; 2019.
[43] Frappa G, Pitacco I, Baldassi S, Pauletta M. Methods to reproduce in-plane deformability of orthotropic floors in the finite element models of buildings. Appl Sci 2023;13(11). article number 6733. doi: 10.3390/app13116733.
[44] Di Marco C., Frappa G., Sabbà M.F., Campione G., Pauletta M. Shear strength formula for interior beam-column joints with plain bars in existing buildings. Engineering Structures 293,116656.
[45] Hakuto S, Park R, Tanaka H. Seismic load tests on interior and exterior beam-column joints with substandard reinforcing details. ACI Struct J 2000;97(1):11–25.